Palaeogeography, Palaeoclimatology, Palaeoecology 655 (2024) 112486

Contents lists available at ScienceDirect

Palaeogeography, Palaeoclimatology, Palaeoecology

journal homepage: www.elsevier.com/locate/palaeo

Climate, vegetation, and environmental change during the MIS 12-MIS 11 glacial-interglacial transition inferred from a high-resolution pollen record from the Fucino Basin of central Italy

Pablo Vera-Polo [a,b,*], Laura Sadori [a], Gonzalo Jiménez-Moreno [b], Alessia Masi [a], Biagio Giaccio [c,d], Giovanni Zanchetta [e], P. Chronis Tzedakis [f], Bernd Wagner [g]

[a] Dipartimento di Biologia Ambientale, University of Rome "La Sapienza", Rome 00185, Italy
[b] Departamento de Estratigrafía y Paleontología, Universidad de Granada, Granada 18071, Spain
[c] Istituto di Geologia Ambientale e Geoingegneria, CNR-IGAG, Monterotondo, Rome 00015, Italy
[d] Istituto Nazionale di Geofisica e Vulcanologia, INGV, Rome 00143, Italy
[e] Dipartimento di Scienze della Terra, University of Pisa, Pisa 56126, Italy
[f] Environmental Change Research Centre, Department of Geography, University College London, London WC1E6BT, UK
[g] Institute of Geology and Mineralogy, University of Cologne, Cologne 50939, Germany

ARTICLE INFO

Editor: H. Falcon-Lang

Keywords:
Pollen analysis
Mediterranean region
Central Italy
Glacial-interglacial cycles
MIS 12
Termination V
MIS 11c
Climate change
Mid-Brunhes Event

ABSTRACT

Glacial Termination V (T-V) comprised a relatively rapid shift from glacial to interglacial conditions (MIS 12 glacial to the MIS 11c); it was one of the greatest climatic changes of the Pleistocene, and forms part of the major climatic reorganization known as the Mid-Brunhes Event (MBE). The Fucino Basin, located in the Central Apennine chain of central Italy, contains a continuous and well-preserved lacustrine sedimentary record of T-V and MIS 11, dated using tephrochronology. In this paper, we report a high-resolution palynological analysis, supported by geochemical proxies, from the lowermost section of the F4-F5 composite record, to improve understanding of T-V in this region. This record reveals a substantial transition between MIS 12 and MIS 11c at 424.5 ± 4.0 ka, from a very cold and dry environment indicated by the herbaceous and xerophytic association of Poaceae, *Artemisia*, Amaranthaceae, *Ephedra*, and *Hippophäe*, and sedimentation dominated by inorganic siliciclastic sediments, to a warm and humid period characterised by a significant increase in *Abies* and a deciduous tree association mainly formed by *Betula, Carpinus*, *Corylus, Quercus*, *Ulmus,* and dominated by more organic calcareous sediments. This transition was correlated with a significant lake-level rise, with an enhanced nutrient input into the lake between 425.0 ± 4.5 ka and 424.0 ± 3.9 ka, as inferred from the variance between algae, aquatic plants, and terrestrial herbaceous taxa. Following the MIS 11c temperature maximum at 424.2 ± 3.9 ka, a reduction in summer insolation occurred, provoking a significant increase in humidity that produced the widespread development of *Abies*. The results from this study suggest that, at Fucino, fluctuations in humidity are predominantly responsible for the vegetation changes observed during T-V.

1. Introduction

The Quaternary climate is characterised by a marked periodical alternation of glacial and interglacial (G/I) cycles, paced by Earth's orbital parameters changes (Hays et al., 1976). Studying temporally long paleoecological records is crucial for understanding recurrent climatic and paleoenvironmental changes, such as G/I cycles, but also for exploring unique aspects among them (Tzedakis and Bennett, 1995; Tzedakis, 2007; Tzedakis et al., 2009).

One notably long interglacial was MIS 11c (~426–396 ka) (Tzedakis et al., 2022), which spanned two precessional cycles and was marked by high sea levels (6–13 m above present; Spratt and Lisiecki, 2016) and high atmospheric greenhouse gases concentration (hovering around 265–280 CO_2 ppm for ~30 kyr; Brandon et al., 2020; Nehrbass-Ahles et al., 2020). Its low-amplitude precessional changes and subdued insolation variations, a result of the 400-kyr eccentricity cycle (marked by low present eccentricity values), make it a partial astronomical analogue for the Holocene (Loutre and Berger, 2000; Tzedakis, 2010).

* Corresponding author at: Dipartimento di Biologia Ambientale, University of Rome "La Sapienza", Rome 00185, Italy.
E-mail address: pablo.verapolo@uniroma1.it (P. Vera-Polo).

https://doi.org/10.1016/j.palaeo.2024.112486
Received 21 June 2024; Received in revised form 2 September 2024; Accepted 2 September 2024
Available online 4 September 2024

MIS 12 was characterised by one of the largest glaciations registered in Europe (Ehlers and Gibbard, 2008). The end of this glacial period (Termination V) seems to occur when the insolation values began to rise, coinciding with a large volume of ice covering the Earth surface (Raymo, 1997). Glacial Termination V (T-V), which occurred between 430.5 ± 1.5 and 426.0 ± 2.0 ka (Cheng et al., 2016), is consequently recognised as one of the most extreme climatic shifts in the last 900 ka of the Earth system, despite minimal astronomical forcing (Napier et al., 2018; Giaccio et al., 2021; Sassoon et al., 2023). This large climatic change is also known as the Mid Brunhes Event (MBE), which marks the definitive establishment of the long, high-amplitude, and saw-tooth structured G/I cycles (Berger and Wefer, 2003). While the insolation forcing during T-V was relatively weak (Loutre and Berger, 2000), it was associated with one of the highest-amplitude deglacial warmings (Berger and Wefer, 2003; Rodrigues et al., 2011). This rapid climate warming provoked one of the biggest increases in global biosphere productivity, reaching values of 10–30 % higher than present-day (according to pollen data and total organic carbon; Brandon et al., 2020). The disparity between the modest insolation forcing and the pronounced climatic response is known as the "Stage 11 problem" (Imbrie et al., 1993). Tzedakis et al. (2022) suggested that the weak forcing led to a slow deglaciation that continued well into MIS 11c, but constraining the rate of the sea-level rise is challenging (Rohling et al., 2010; Vázquez Riveiros et al., 2013; Barker et al., 2015). Independently dated records are crucial for assessing these paleoclimatic questions and identifying short- and long-term paleoclimatic changes and their drivers (e.g. Bakker et al., 2017; Li et al., 2023; Leicher et al., 2024) and could be helpful to solve this "Stage 11 problem".

The Mediterranean region, with its complex interplay of tectonics, volcanism, and thick lacustrine sedimentary sequences provides a unique setting to investigate the dynamics of G/I cycles (Tzedakis et al., 1997). Mediterranean pollen records provide valuable insights into the region's vegetation and climatic history. In addition, due to the proximity of the studied Mediterranean pollen sites (e.g., in Balkan Peninsula, Koutsodendris et al., 2019, 2023a; Donders et al., 2021) to refugial areas (any area of any size in which a taxon persisted at any population density during a cold stage; Bennett et al., 1991) it is postulated that there are no significant migrational lags in the Mediterranean pollen records (Magri and Tzedakis, 2000). Because of this, the Mediterranean region is characterised by a wide variety of landscapes, including treeless areas, woodland and several types of forests, with the occurrence of typically Mediterranean adapted plants or mesophilous trees. This vegetational variability allowed us to find representations of diverse climatic associations in relatively small areas and study their response to climate changes throughout time.

The Fucino Basin, in central Italy (Fig. 1), is the largest and, possibly, oldest and long-lived basin of the Central Apennines intermountain tectonic depressions system (e.g. Cavinato et al., 2002), whilst the entire lacustrine sedimentary succession of the Fucino Basin could continuously span back to 2 Ma (Giaccio et al., 2015). The hitherto well investigated uppermost interval contains the richest and most continuous Mediterranean succession of well-documented and radioisotopically dated Middle to Upper Pleistocene volcanic layers (tephras), enabling an accurate and precise age model for the last 424 ka (Giaccio et al., 2017, 2019; Monaco et al., 2021, 2022; Leicher et al., 2023, 2024), and may span the last 430 ka (e.g. Giaccio et al., 2019).

In this study, we present a detailed pollen record from the lowermost portion of this record, spanning the end of MIS 12 and the beginning of MIS 11. The high-resolution pollen data allow us to study millennial-scale vegetation changes and to gain insight into the significant environmental change and climatic fluctuations that occurred during the MBE.

2. Study site: geology, climate, and vegetation

The Fucino Basin (42° 00′ N; 13° 30′ E) is situated approximately at 650 m a.s.l. within the Central Apennine Chain (Abruzzo) and is bounded by mountain peaks such as Monte Velino (2486 m a.s.l.) and Monte Sirente (2348 m a.s.l.). It is the largest (~900 km^2) Central Apennine intermountain tectonic basin, hosting thick and continuous Plio-Quaternary alluvial and lacustrine deposits (Cavinato et al., 2002; Giaccio et al., 2019) (Fig. 1). The basin opened during the post-orogenic tectonic extensional phase along the Fucino Fault System (FFS), which has been active since the Pliocene and consists of three principal segments oriented along a 110°-140°N axis (Galadini and Galli, 2000; Cavinato et al., 2002; Galadini and Messina, 2004; Mondati et al., 2021). The FFS activity and configuration, consequence of the general regional uplift, resulted in the formation of a half-graben basin with a steep topographic slope on the basin floor (Giaccio et al., 2015; Caielli et al., 2023). Lake Fucino formed at the lowermost part of the basin during the Early Pleistocene, occupying an area of ~140 km^2 and reaching a maximum water depth of 20 m, being the Italy's third largest lake (Mannella et al., 2019), before its artificial drainage in 1875 for agricultural purposes (Giaccio et al., 2017),. The interaction between the lake and the differential movements along the FFS controlled the sedimentary infilling of the basin. This resulted in a presumably continuous deposition, with a variable sedimentation rate, and influenced by the wedge-shape sedimentary infilling forced by the basin's half-graben geometry (Giaccio et al., 2017, 2019; Mannella et al., 2019), of fine-grained lacustrine calcareous marls, fluvio-glacial sediments from the surrounding relief, and several tephra layers from peri-Tyrrhenian magmatic provinces (Giaccio et al., 2017, 2019; Monaco et al., 2021, 2022; Leicher et al., 2023, 2024). As a result, Quaternary deposits of ~900 m accumulated in the depocenter, with increasing sedimentation rates from west to east.

At present, the Fucino Basin is characterised by a Mediterranean climate with warm and dry summers (e.g. Lionello et al., 2006) and continental characteristics, according to historical data from the regional meteorological network (Peyron et al., 2013) and from data recollected from the nearby Borgo Ottomila meteorological station (652 m a.s.l.). From April to October, monthly average temperatures are over 10 °C, peaking in July and August (18 to 21 °C). From November to March, monthly average temperatures are below 10 °C, with January being the coldest month recording minimum daily temperatures from −5 to −2 °C (Mannella et al., 2019). The WorldClim v2.1 database (Fick and Hijmans, 2017) recorded present-day mean annual temperatures of ~10.0 °C, however, according to the information from meteorological stations, the mean annual temperature for Fucino Basin is ~12.5 °C. The average annual precipitation ranges from 600 to 750 mm in the plains to 900 to 1200 mm in the piedmont zone.

Due to the unique lithological and geomorphological setting of the Fucino Basin, mountain and Mediterranean climates are represented in the same region, controlling the vegetation distribution. This makes the central Apennines a region with a rich and diverse vegetation, characterised by a complex mosaic of vegetation zones (Fig. S1) and different from that of central Europe, being more related to the vegetation of south-eastern Europe (Blasi and Del Vico, 2012). The present-day potential natural vegetation in the area is difficult to identify because of significant human impact and agricultural use (Frate et al., 2018). The vegetation in the Fucino Basin is currently dominated by grasslands on the lower and flatter areas of the basin and extends to the western side of the surrounding reliefs, due to the pluviometric shading caused by the predominantly westerly winds (Tomassetti et al., 2003). The potential natural vegetation in this area is dominated by hygrophilous and hydrophytic freshwater vegetation (Blasi et al., 2017) at the lowermost part of the basin. At lower elevations at the base of the surroundings reliefs, oak forest with *Quercus pubescens* dominates. Mixed woods of *Ostrya carpinofolia*, *Quercus cerris*, and *Acer* spp. spread in cooler and higher elevation areas (Fig. S1). Communities of evergreen scrubs dominated by *Quercus ilex* are established in thermally favourable areas and on lithoid outcrops. At the lower limit of the mountain plain, in the valleys and ravines, grows a mixed forest linked to particularly riparian

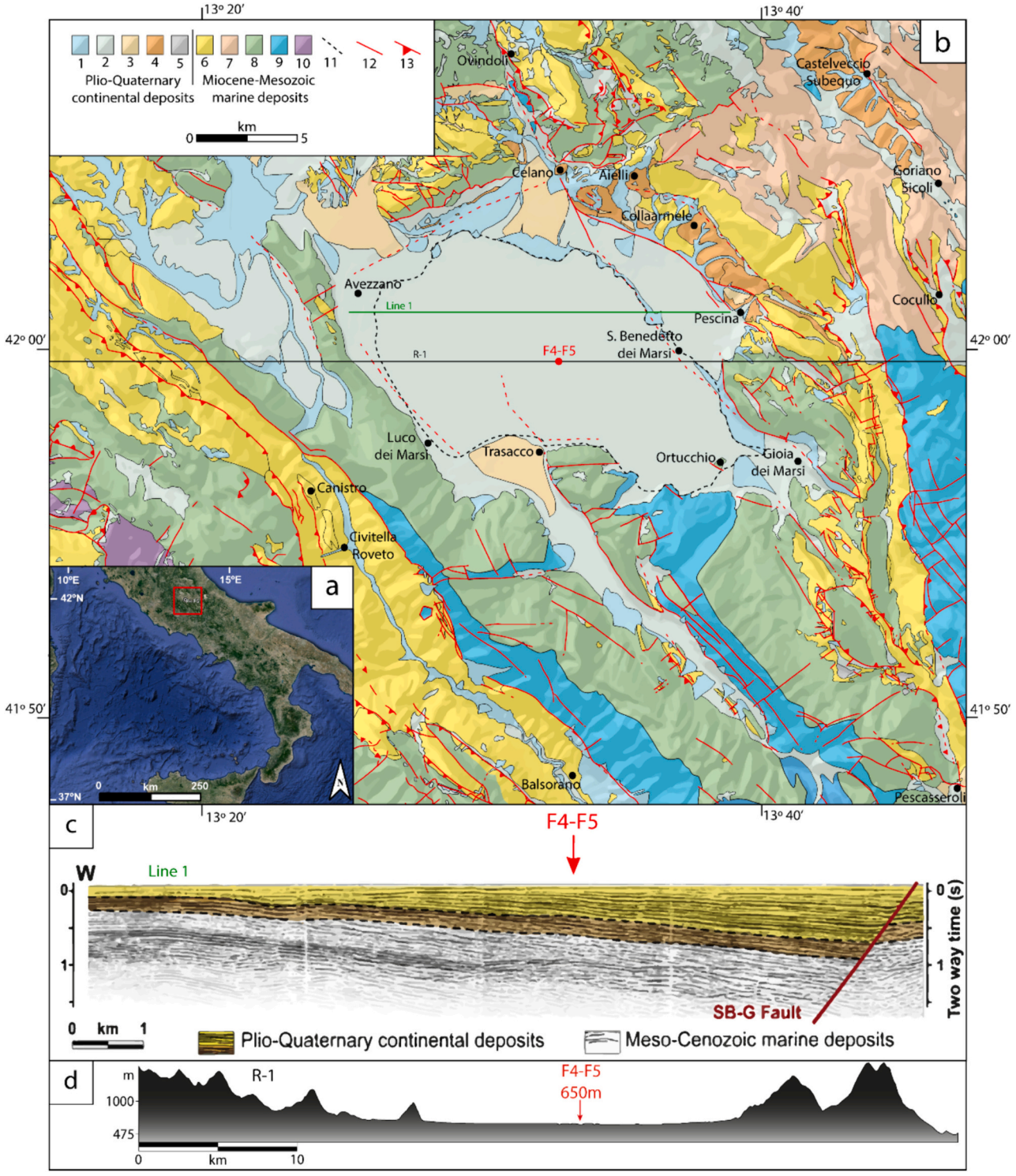

Fig. 1. a) Geographical location of the Fucino basin (red square) in Italy. Image obtained from Google Earth. b) Simplified geological map of the basin area. Modified from ISPRA, 1934, 1939, 1942, 1967 and Caielli et al., 2023. 1) Holocene-Upper Pleistocene calcareous debris fans and fluvio-lacustrine conglomerates; 2) Holocene fluvio-lacustrine deposits; 3) Middle-Upper Pleistocene talus and alluvial fans; 4) Middle Pleistocene calcareous lacustrine deposits. 5) Pleistocene moraine deposits; 6) Miocene brackish marls, sandstones, conglomerates and calcarenites from carbonate ramp; 7) Eocene stratified limestones with Nummulites; 8) Cretaceous well-stratified calcareous and dolomitic series from platform and margin; 9) Jurassic calcareous dolomitic banks with gastropods and brachiopods; 10) Triassic dolomitic series. 11) Historical lake margin (Holocene); 12) Fault and normal faults 13) Thrust faults. Simplified shaded relief is used as basemap to highlight the morphological configuration of the basin. c) Seismic Line 1 (see green trace in panel b) depicting the architecture of Plio-Quaternary continental deposits in the Fucino Basin along a W-E orientated profile, from Giaccio et al., 2019. d) Relief around the Fucino Basin following the black trace R-1 from the panel b). Altitude in m.a.s.l. (For interpretation of the references to colour in this figure legend, the reader is referred to the web version of this article.)

conditions, with *Acer pseudoplatanus, Ulmus glabra, Tilia platyphyllos* and *Fraxinus excelsior*. The mountain bioclimatic vegetation belt is dominated by *Fagus sylvatica*, flanked, in some locations as isolated stands, by *Abies alba*. The rich floral array of beech forests differs, depending on the type of substrate and climatic conditions, giving the development of various plant associations (Fig. S1). Small forest patches of *Betula pendula,* a glacial relic, complement the vegetation panorama and confirm the importance of the basin for conservation of biodiversity. Above 2000 m forests give way to less dense formations, with herbaceous plants becoming the undisputed protagonist of the high mountain vegetation, which is rich in endemic taxa and glacial relics. The alpine meadows, rocky slopes, and scree fields with a vegetation dominated by Poaceae, Cyperaceae, and alpine herbs are adapted to alpine mountainous conditions (Blasi et al., 2010; Blasi et al., 2017) (Fig. S1).

3. Materials and methods

3.1. The composite F4-F5 core

Two parallel holes, F4 and F5, taken approximately 3 m apart, were drilled in June 2017 in the central area of the basin (42°00′07″ N, 13°32′19″ E; Fig. 1; Giaccio et al., 2019) with a 1.5-m-long core barrel and 0.75 m overlap between succeeding runs in both holes to continuously recover the entire sedimentary succession. Cores F4 and F5 reached depths of 87.00 m and 87.75 m, respectively. The composite F4-F5 record was built by establishing correlations between the lithological and physical properties of the individual cores from parallel holes. This overlap minimized any potential gap that could have occurred between subsequent core sections from the two holes (Giaccio et al., 2019). This study is restricted to the bottommost part of the record and includes only the sediment succession recovered in the lowermost core barrel of the F5 hole, without the possibility of establishing a direct correlation with the F4 core (Fig. 2).

3.2. Geochronology and age-depth modelling

The F4-F5 composite record contains at least 130 tephra layers (Giaccio et al., 2019), which allow a precise geochronological analysis for different stratigraphical intervals spanning the last ~430 ka (Giaccio et al., 2017; Monaco et al., 2021, 2022; Leicher et al., 2023, 2024).

The analytical details of the chronological control for the investigated interval were previously described by Monaco et al. (2021). Specifically, the age model for the ~365–430 ka interval and related 95 %-confidence interval were both generated using the open-source statistical environment R (R Core Team, 2017) and the Bacon programme (Blaauw and Christen, 2011), which was constrained by 9 tephra layers dated directly or indirectly with the $^{40}Ar/^{39}Ar$ method (Monaco et al., 2021) (Fig. 2).

The age model provided by Monaco et al. (2021) extrapolated the sedimentation rate between the lowermost two tephra layers (TF-125, 414.8 ± 2.2 ka and TF-126, 424.3 ± 3.2 ka) towards the bottom of the sediment succession. However, a distinct lithological change, clearly documented by the XRF Ca data (Fig. S2; Monaco et al., 2021) at 97.30 m composite depth, ~5.6 cm below TF-126 marks the transition from MIS 12 glacial sedimentation below to MIS 11c interglacial sedimentation above (Monaco et al., 2021). As the average sedimentation rates in the F4-F5 core during the following glacial periods MIS 10, MIS 8, MIS 6, and MIS 4–2 range between 0.12 and 0.28 mm/yr (Giaccio et al., 2019; Monaco et al., 2021, 2022; Leicher et al., 2023, 2024), we here extrapolated a mean sedimentation rate of 0.20 mm/yr for the section below 97.30 m, with a propagated uncertainty of 3.5 ka to 5.0 ka, which also accounts for the range of variability of sedimentation rate (Fig. 2).

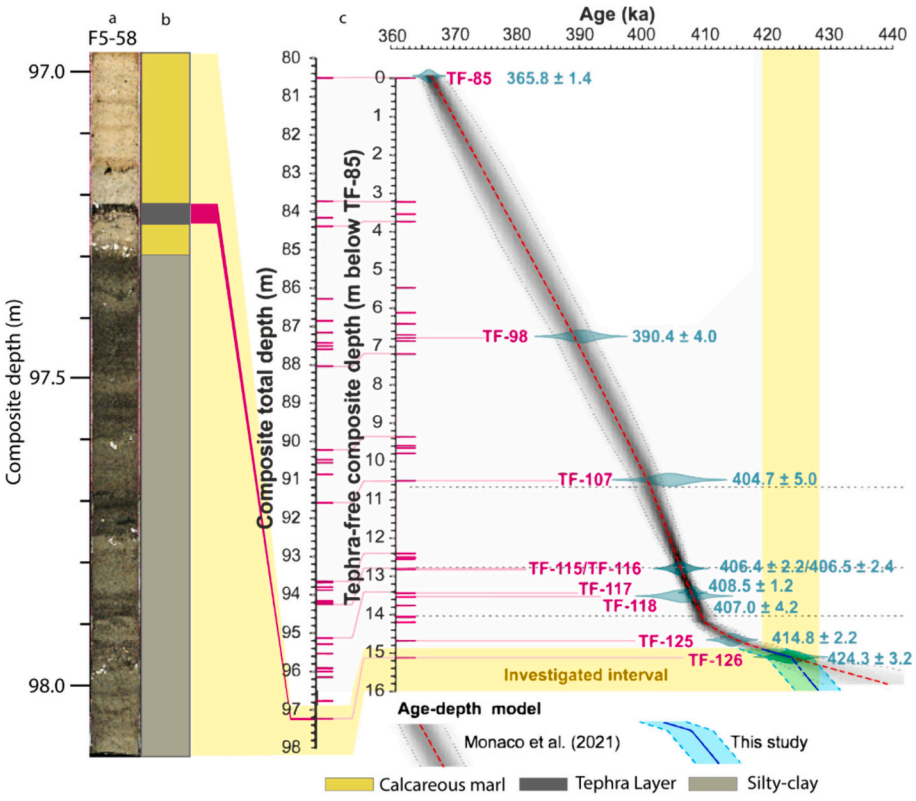

Fig. 2. a) Core-scanner image of the core-section F5–58; b) Simplified lithology of the core section F5–58. c) Bayesian age-depth model modified after Monaco et al. (2021) for the 18 m of the composite core interval. The yellow rectangle represents the interval investigated here (418–428 cal. ka). The pink marks are the tephra layers identified along the core. From 424.3 (TF-126) to the base the age model for this study was changed in comparison to the previous age extrapolation (Monaco et al., 2021; see text for details). (For interpretation of the references to colour in this figure legend, the reader is referred to the web version of this article.)

Overall, the resulting age-depth model provided age constraints with an overall uncertainty of ±4.2 ka, ranging from 3.6 ka to 5.0 ka. As a result, samples ages encompassing an age range between 429.0 ± 5.0 ka to 418.5 ± 3.6 ka in the record are derived from this extrapolation.

3.3. XRF

X-ray fluorescence (XRF) scanning was conducted on the split core halves of the F4-F5 sediment cores using an ITRAX XRF scanner (Cox Analytical Systems, Sweden) with a line-scan camera mounted and a chromium tube set at 55 kV and 30 mA, a dwell time of 10 s and a step-size of 2.5 mm. The resulting data were processed using the QSpec 6.5 software (Cox Analytical, Sweden), and the values are presented in counts per second, averaged at 25 cm intervals. So far, only Ca counts from the analysis were published (Giaccio et al., 2019). The optical information obtained from the high-resolution line-scan imaging and XRF data were used to correlate the individual overlapping core segments from F4 and F5 sites (see Giaccio et al., 2019 for details).

To gain more information about the past environmental and sedimentary conditions, 13 elements of the XRF data were used, including calculation of the following ratios, which proved to be useful for Fucino Basin.

- Zr/K: It determines grain size changes (Cuven et al., 2011). Zr is very resistant to weathering and transport and is usually enriched in coarse sediment fractions (Wang et al., 2011; Croudace and Rothwell, 2015), whereas K is associated with illite clays and feldspar, and is more common in fine grained sediments (Kuhlmann et al., 2004). So, higher values of this proxy represent a coarser grain size composition.
- Ca/Ti: We adopted this ratio because the origin of Ca, in the Fucino Basin, is ambiguous and can be the result of in situ endogenic carbonate precipitation, or, to a minor extent, of biogenic shell calcification such as in ostracods, or of detrital influx from the large outcrops of marine limestones (Mannella et al., 2019). Endogenic carbonates precipitate due to the decrease of dissolved CO_2 from warmer water temperatures or photosynthesis (Freytet and Verrecchia, 2002). In this context, Ca/Ti would then mostly express authigenic carbonate precipitation without detrital input, being Ti only of clastic origin.
- Si/Ti: It is used as a proxy to determine siliceous productivity (biogenic silica) (e.g. Stansell et al., 2010; Brown, 2011; Melles et al., 2012).

The Log ratios were used to address and minimize any core scanner detector drifts, dilution effects and sources of irritation, providing the most robust record of relative chemical changes in the sedimentary record and reducing interpretation risks (Croudace and Rothwell, 2015).

A Principal Components Analysis (PCA) was performed on the XRF data using the Past4 software (Hammer et al., 2001), removing the data that corresponds with the tephra layer, in order to avoid that the geochemical associations connected to specific sedimentation processes (e.g., erosion and productivity) may be affected (Fig. S2). The PCA allows for the identification of variables (components) that capture the majority of variance within multivariate data (Hammer et al., 2001).

3.4. Geochemical analyses on discrete samples

Discrete samples taken from the top of each core catcher and every 4 cm were processed for total carbon (TC) and total inorganic carbon (TIC), and stable carbon and oxygen isotopes (see Mannella et al., 2018 for details). TOC was calculated from the difference of TC and TIC and used for this study, along with $\delta^{18}O$ for the paleoclimatic interpretations.

3.5. Pollen analysis

The palynological study focuses on T-V and the G/I transition within the deepest part of the F4-F5 record (drive F5–58). The age model modified from Monaco et al. (2021) (Fig. 2) was taken into consideration when selecting samples for this study. The sampling strategy involved three distinct intervals: 4-cm intervals (the bottommost 44 cm), 2-cm intervals (the overlying 28 cm), and 1-cm intervals (the uppermost 35 cm), excluding the tephra layers. This approach was used to compensate the presumed changes in sedimentation rates, with the aim of achieving a high-resolution record for the studied period. Consequently, a total of 66 samples were obtained, with a range of temporal spacing between samples of ~50 and ~ 215 years, resulting in an average temporal resolution of ~200 years between individual samples. After freeze drying, the samples were treated with hydrochloric acid (HCl, 37 %) to remove carbonates, hydrofluoric acid (HF, 48 %) to remove silicates, and sodium hydroxide (NaOH, 10 %) to eliminate the cellulose fraction with the goal of concentrating the organic matter. A tablet of *Lycopodium* spores was added to each sample to calculate pollen concentrations. Subsequently, the samples were sieved using a 10 μm nylon sieve to remove particles smaller than pollen grains, including clays. The remaining material was mounted on microscope slides using glycerine. Palynomorph identification was performed under transmitted light microscopy at 400× magnification. Most of the samples showed abundant pollen grain concentrations, allowing the identification of a total of 300 terrestrial and aquatic pollen grains per sample. However, eighteen samples, from the lowermost interval (between 98.02 and 97.27 m composite depth; Fig. 3a), were characterised by such low pollen concentrations that counts of 300 pollen grains were not possible. These samples provided between 170 and 266 pollen grains, being mostly above 200. Overall, the pollen quantities proved to be sufficient for making a broadly environmental interpretation (Djamali and Cilleros, 2020).

Pollen grains identified as cf. *Juniperus* (Fig. 3) may include some grains of other Cupressaceae such as *Cupressus*, as well as those of *Taxus*. The last two were not observed in the samples, but we cannot exclude their presence in some of the pollen samples, considering the poor state of preservation of those pollen grains, primarily in the MIS 12 glacial samples, when *Juniperus* ss. was rather abundant.

The percentages of the different pollen taxa were calculated and represented using the Tilia Software, version 2.6.1 and an objective zonation of the pollen data was performed using CONISS cluster analysis (Grimm, 1987; Fig. 3). This software was used to compute the concentration of pollen grains in samples (Fig. 3a), considering the mass quantity (~2 g per sample) and the number of *Lycopodium* spores added and counted for each sample. The percentage of Non-Pollen Palynomorph (NPP) was calculated in relation of the total sum of the total pollen amount plus the total NPP.

In addition, a PCA was performed on both pollen and NPP percentage data. For comparison, the PCA was conducted to reduce the dataset to two variables (the first two components) (Fig. 4).

According to former studies (e.g. Joannin et al., 2011; Bertini et al., 2015; Camuera et al., 2019) and to PCA results (Fig. 4), pollen grains were grouped into ecologically-significant specific vegetation categories such as xerophyte/steppe taxa (*Artemisia,* Amaranthaceae*, Ephedra, Hippophaë*), altitudinal taxa (*Abies, Betula, Cedrus, Fagus, Picea, Tsuga*), and mesothermic taxa (*Acer*, *Alnus*, *Buxus, Carpinus betulus*, *Carpinus orientalis/Ostrya*, *Carya*, *Celtis,* Cistaceae, *Corylus*, Ericaceae, *Fraxinus*, *Hedera*, *Juglans*, *Olea*, *Pistacia*, *Phillyrea*, *Pterocarya*, *Quercus* total*, Salix, Tilia, Ulmus, Zelkova*) (Figs. 3 and 5). Due to their low abundance, the correlation analysis, and according to PCA results (Fig. 4a), the Mediterranean/sclerophyllous taxa (Cistaceae, *Fraxinus*, *Olea*, *Pistacia*, *Phillyrea* and *Quercus* evergreen) were included in the group of mesothermic taxa (Fig. 5). The aquatic plants were excluded from the total sum of pollen. These categories have been shown to be successful as trustworthy climatic proxy indicators in the Mediterranean region

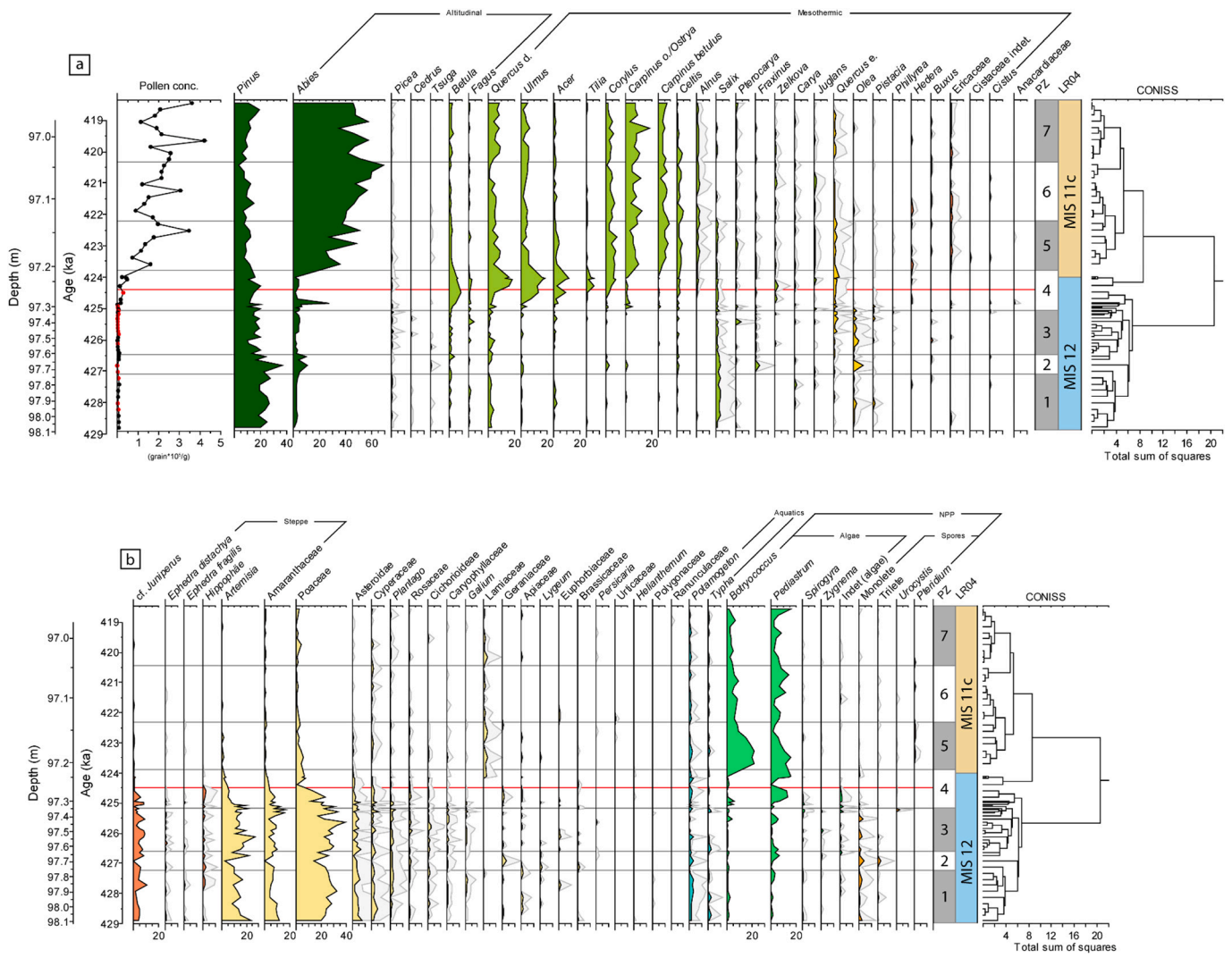

Fig. 3. Detailed percentage pollen diagram from the F4-F5 record. Total pollen concentration is shown in the first curve of the uppermost diagram (3a) followed by trees and shrubs. Red dots in pollen concentration curve indicates the samples that didn't reached the 300 pollen grains counts. Dark-green: coniferous trees; yellow-green: deciduous trees; yellow: sclerophyllous trees; orange-red: shrubs. In the lowermost diagram (3b) are displayed: herbaceous: pale-yellow; aquatic: turquoise; algae: light-green; spores: orange; other Non-Pollen Palynomorphs (NPP): black and the cluster analysis done by CONISS (Grimm, 1987). The boundary between MIS 12 and MIS 11 suggested by Lisiecki and Raymo (2005) is shown by the blue and beige boxes at ~424 ka. The red line indicate the Glacial-Interglacial boundary suggested by pollen zones (PZ) and CONISS analysis for the F4-F5 composite record. The light grey shading in the pollen percentages represents an exaggeration of the abundance x5. (For interpretation of the references to colour in this figure legend, the reader is referred to the web version of this article.)

(Altolaguirre et al., 2020).

3.6. Quantitative paleoclimatic reconstruction

A paleoclimatic quantitative reconstruction (mean annual precipitation and temperature) of the Fucino Basin pollen data was done using the C2 software (Juggins, 2007), integrating the Eurasian Modern Pollen Database (EMPDv2) and the paleoclimatic parameters from WorldClim v2.1 database (Fick and Hijmans, 2017) (Figs. 6, S3, S4 and S5). This comparison was made using a non-linear unimodal technique, Weighted-Averaging Partial-Least Squares (WA-PLS) regression. This type of model assumes that plant species have their maximum abundances in different climate niches and that niche breadth drives the species environmental tolerance (Chevalier et al., 2020). To reduce noise, the square-root species transformation was applied to the pollen training set for the pollen-based transfer function. For the construction of WA-PLS regressions, a total of five components were run, however, we used the second component (2C) WA-PLS model under the leave-one-out cross-validation method. Increasing the number of components reduces the root mean squared error, but it can also result in overfitting the data, resulting in a drop of the model predictive value (Camuera et al., 2022; Ter Braak and Juggins, 1993). After this analysis, the results of the coefficient of determination (R^2) were obtained, which determines the reliability of each of the reconstructions (Fig. S3). The closer this value is to 1, the more reliable it is (Ter Braak and Juggins, 1993). One difference between the quantitative WA-PLS and the qualitative PCA is that the WA-PLS assumes that the parameters to be estimated are fixed and the data are random observations from some population (Ilvonen et al., 2022), whereas the PCA uses arbitrary initial site scores without environmental parameters (Ter Braak and Juggins, 1993).

We also estimated the relative lake-level changes (Fig. 7) taking the formula used in Camuera et al. (2019): Algae total/(Algae total + Aquatic plants + Poaceae). However, this "lake level" qualitative estimation, primarily based on the amount of algae, also depends on trophic conditions of the lake waters and changes in lake bottom morphology.

The Past4 software (Hammer et al., 2001) was employed to determine the correlation between the reconstructions and the pollen data by an univariate correlation analysis, resulting in two statistical values for

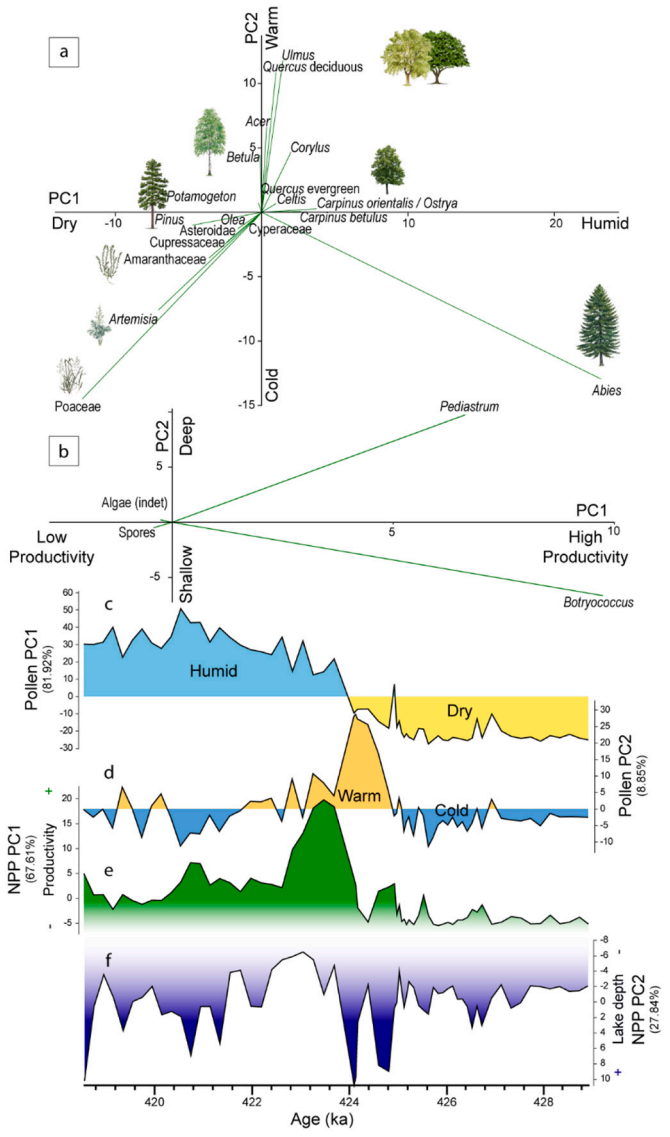

Fig. 4. Principal Component Analysis (PCA) of pollen percentage and Non-Pollen Palynomorphs (NPP) results. (a) Pollen scatter biplot using the PC1 and PC2 with its paleoclimatic interpretation. (b) NPP scatter biplot using the NPP-PC1 and NPP-PC2 with its interpretation. (c) Pollen PC1 is interpreted as the variation in humidity with yellow colour representing the drier period and blue colour the humid one. (d) Pollen PC2 is interpreted as the change in temperature with orange colour (representing the warmest periods) and blue colour (for the colder ones). (e) NPP-PC1 interpreted as the productivity in the lake during the studied period. f) NPP-PC2 inverted interpreted as the lake depth. The analyses were carried out using PAST 4.11 (Hammer et al., 2001). Pollen and NPP taxa with an abundance lower than 1 % and with loadings lower than 0.025 were removed from (a) and (b) diagrams in order to enhance readability. (For interpretation of the references to colour in this figure legend, the reader is referred to the web version of this article.)

each pollen and reconstruction, the correlation value (R; a value between 1 and − 1 representing a positive or an inverse correlation between the variables) and the statistical significance (p; a value near 0 means that the correlation between the variables is statistically significative, being negligible values higher than 0.05). Every value of R shown in this study has statistical significance. This software was used also for smoothing the reconstructed precipitation and temperature signals (Fig. 6) by LOESS modelling with a value of 0.2.

4. Results

4.1. Geochemistry

The XRF analysis provided 462 data points showing substantial changes at the T-V (Fig. S2). The age-related fluctuations of the elements can be separated into three intervals:

1) Prior to 424.9 ± 4.4 ka: Si, K, Ti, Fe, Rb and Zr have high constant values, whereas Ca has lower values (Fig. S2). The Log(Si/Ti) follows the same pattern as the Log(Ca/Ti) but the fluctuations have a higher amplitude (Fig. 7).
2) Between 424.9 ± 4.4 and 423.8 ± 3.8 ka: A transition occurs in which the high values of Si, K, Ti, Fe, Rb and Zr decrease (reverse trend in Ca). During this period, the minimum in Ca and maxima in siliciclastic elements (Fig. S2) is caused by the deposition of tephra TF-126 (Monaco et al., 2021).
3) After 423.8 ± 3.8 ka: the concentrations of Ca persist at elevated levels, exhibiting a slight upward trend, whereas Si, K, Ti, Fe, Rb, and Zr demonstrate a marked decline reaching their respective minima. The Log(Zr/K) increased, maintaining relative constant values along this period (Fig. 7).

The PCA separated the XRF data into two groups. Positive PCA values correspond to Ca and negative values to siliciclastics (Fig. S2). From ~429 to ~425 ka the siliciclastic input increases with respect to the rest of the studied MIS 12. During MIS 11c, the terrigenous input was substituted for Ca-rich sediments.

The TIC from the discrete samples shows an increase between 424.9 ± 4.5 and 423.8 ± 3.8 ka very similar to the XRF Ca data (Fig. 7). During the glacial period (before ~424.5 ± 4.0 ka), TIC values are around 5 % and increase after G/I transition to 8–9 %, which corresponds to ~70 % calcite. TOC shows a similar trend, with values below 1 %, during the glacial and values exceeding 2 % after the transition This patter is also shown in $\delta^{18}O$, with more negative values until ~425 ka and less negative but fluctuating values after the transition (Fig. 7).

4.2. Pollen analysis

Microscopic examination of the samples from the F4-F5 sedimentary record revealed the good preservation of palynomorphs, with the identification of 58 pollen and 13 NPP taxa. The lower 34 samples (corresponding to MIS 12) are characterised by a high detrital content and have much lower pollen concentrations (~5300 pollen grains/g as average concentration value) than the upper 32, carbonate-rich samples (corresponding to MIS 11c, with ~168,000 pollen grains/g as average concentration value) (Fig. 3a).

Herbs such as Poaceae, *Artemisia*, Amaranthaceae, and Asteraceae (mainly Asteroideae) dominated the terrestrial landscape during MIS 12 (Fig. 3). The rare forest taxa that characterised the surroundings of the Fucino Basin during the MIS 12 glaciation were primarily *Pinus* and cf. *Juniperus*, with some deciduous species such as *Quercus* and *Salix*. After T-V, open vegetation was completely replaced by forest species, primarily deciduous trees, such as *Quercus*, *Betula*, *Carpinus*, *Corylus*, *Ulmus*, *Acer* and *Abies*. Within the lake, *Pediastrum* and *Botryococcus* algae also increased during the beginning of MIS 11c (Fig. 3).

The PCA of the pollen data shows that PC1 represents 81.9 % of the total variance of the data, whereas PC2 represents 8.9 %. Most taxa have low loadings (less than ±0.05) except for *Abies*, *Carpinus orientalis/Ostrya*, *Carpinus betulus*, *Corylus*, *Ulmus*, Asteroideae, cf. *Juniperus*, Amaranthaceae, *Pinus*, *Artemisia,* and Poaceae. The positive scores from PC1 correspond to deciduous forest, warm-temperate taxa and *Abies*, and the negative ones corresponds to herbaceous taxa, *Pinus* and aquatics (Fig. 4a). Positive values of pollen PC1 mostly occurred after ~425 ka (Fig. 4c). The negative pollen PC2 group included herbaceous taxa and *Abies.* Positive pollen PC2 groups the deciduous forest (Fig. 4a).

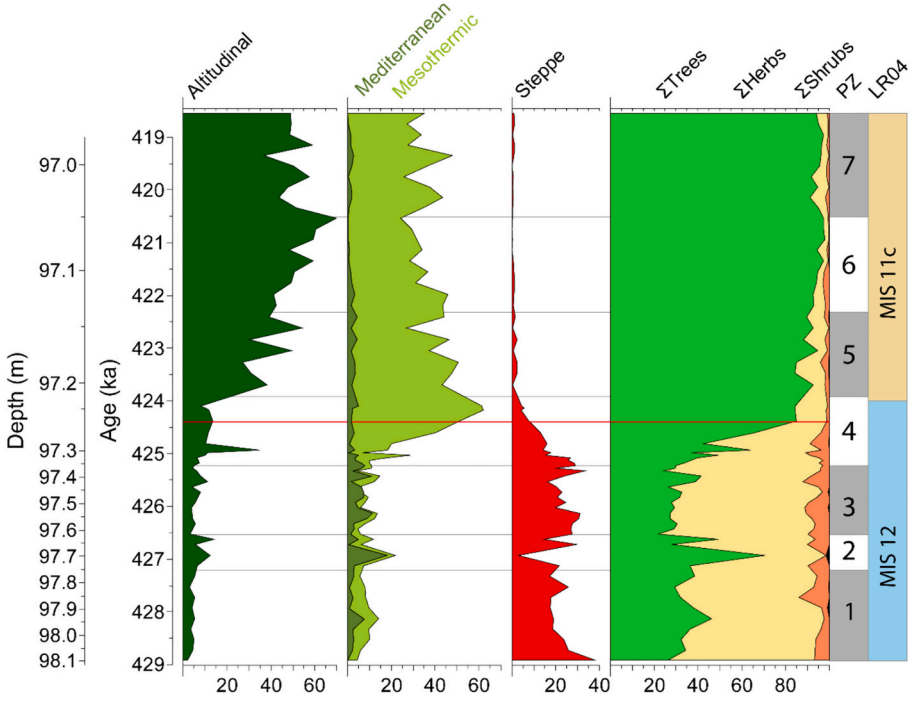

Fig. 5. Terrestrial pollen data grouped into the different paleoecological associations and the different Pollen Zones (PZ) and Glacial-Interglacial F4-F5 boundary (red line) as reference. The boundary between MIS 12 and MIS 11 suggested by Lisiecki and Raymo (2005) (LR04) is shown by the blue and beige boxes at ~424 ka. The taxa lists are reported in the text. (For interpretation of the references to colour in this figure legend, the reader is referred to the web version of this article.)

Most of the values for PC2 were negative, but positive values showed a distinct maximum between ~425 and ~ 422 ka (Fig. 4d).

In addition, a PCA was performed on the NPPs. The NPP-PC1 represents 67.6 % and the NPP-PC2, 27.8 % of the variances. The analysis separates three main groups defined by *Pediastrum* (positive NPP-PC1 and positive NPP-PC2), *Botryococcus* (positive NPP-PC1 and negative NPP-PC2) and the third group dominated by spores (negative NPP-PC1) (Fig. 4b). The evolution of NPP-PC1 over time seems to be related to pollen PC2 with a centennial-scale delay between their maxima and minima (Fig. 4e). The NPP-PC2 shows two main different periods, more stable values, and more abrupt changes, with a boundary at 424.5 ± 4.0 ka.

According to CONISS analysis on pollen data, the pollen diagram was divided into 7 pollen zones (PZ) (Figs. 3 and 5).

4.2.1. PZ-1 (between 428.9 ± 5.0 ka and 427.2 ± 5.0 ka; 98.10–97.76 m)

Herbaceous plants were mainly represented by Poaceae (19.3–31.5 %). Steppic taxa predominated, mainly represented by *Artemisia* (8.6–23.5 %) and Amaranthaceae (3.4–11.1 %). Conifer taxa were dominated by *Pinus* (17.7–27.1 %) and cf. *Juniperus* (1.7–10.4 %). Deciduous tree forest was composed of *Quercus* deciduous type (1.1–4.1 %) and *Salix* (0.3–3.4 %), including some small peaks of *Acer* (0.0–2.3 %) and *Ulmus* (0.0–1.0 %). This subzone had the major representation of aquatic and hygrophilous taxa of all the samples analysed in this study (Cyperaceae: 1.0–4.9 %; *Potamogeton*: 0.8–3.0 %; *Typha*: 0.0–2.3 %).

NPPs rarely occur during this zone.

4.2.2. PZ-2 (between 427.2 ± 5.0 ka and 426.6 ± 5.0 ka; 97.76–97.63 m)

During this period, the steppe taxa decreased drastically and mesothermic taxa colonised the area. There was also an increase in altitudinal taxa, mainly dominated by *Abies* (3.8–10.5 %). The tree forest, dominated by *Pinus* (16.5–35.3 %), *Olea* (0.0–7.5 %), *Salix* (1.9–3.0 %) and *Corylus* (0.0–3.0 %), was more abundant than the herbaceous vegetation. The highest spore concentration occurred in this zone (0.6–6.7 %).

4.2.3. PZ-3 (between 426.6 ± 5.0 ka and 425.1 ± 4.5 ka; 97.63–97.33 m)

Among herbs, Poaceae dominated this period (17.4–38.9 %), followed by the steppe plants *Artemisia* (10.9–26.2 %) and Amaranthaceae (2.6–15.7 %). The tree population was dominated by *Pinus* (9.3–20.0 %) and *Abies* (1.3–5.1 %). The abundance of algae increased. *Quercus* deciduous type decreased during the second half of the zone. There were some levels, mainly at the end of the zone, where dinoflagellate cysts occurred.

During PZ-2 and PZ-3 a surprising increase in grains of *Olea* and *Quercus* evergreen type was found (Fig. 3). We cannot exclude the possibility of reworked pollen for these zones.

4.2.4. PZ-4 (between 425.1 ± 4.5 ka and 423.9 ± 3.8 ka; 97.33–97.22 m)

PZ-4 characterises a transitional period, with the substitution of the steppic (4.0–26.2 %) by mesothermic (6.7–61.0 %) plants, composed by *Ulmus* (0.0–18.0 %), *Quercus* deciduous type (1.2–17.3 %), *Acer* (0.3–12.0 %), *Corylus* (0.0–7.7 %) and *Tilia* (0.0–6.0 %). Whereas the deciduous forest increased substantially, the herbs started to disappear in a more gradual way. The change was marked in terrestrial vegetation by a peak of *Abies* (27.6 %) and, in the aquatic environment, by an increase in *Pediastrum*.

The demarcation between the glacial MIS 12 and the interglacial MIS 11c pollen boundary was established in the middle of this PZ at 424.5 ± 4.0 ka and using a value higher than 75 % Arboreal Pollen (AP) according to Allen et al. (2000) and to the Fucino terrestrial pollen CONISS results.

4.2.5. PZ-5 (between 423.9 ± 3.8 ka and 422.3 ± 4.0 ka; 97.22–97.14 m)

PZ-5 shows a significant increase in pollen concentration. Altitudinal taxa (26.3–54.3 %) dominated by *Abies* (24.7–51.3 %) were the most representative, followed by mesothermic taxa (27.0–49.0 %). *Carpinus* is abundant in this zone as well as in the following PZ-6 and PZ-7, maintaining constant values through time (~8–10 %).

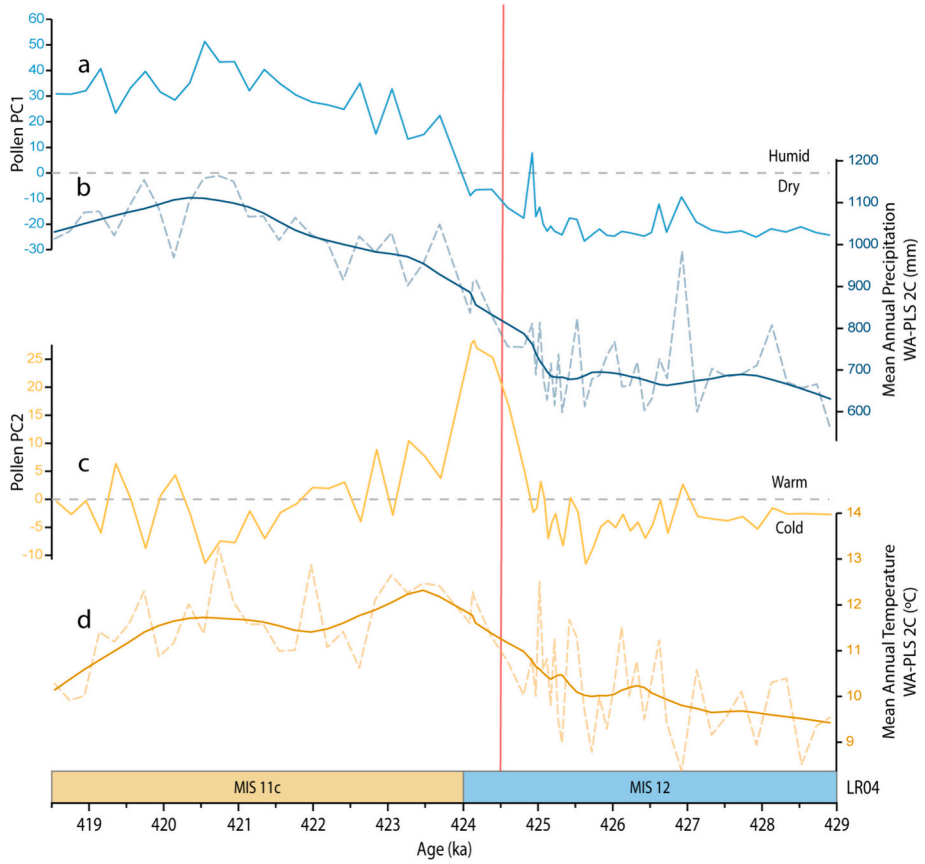

Fig. 6. Comparison of the pollen Principal Component Analysis (PCA) interpretation and the Weighted-Averaging Partial-Least Squares (WA-PLS) 2C reconstruction. a) Humidity reconstruction from Pollen PC1. The dashed line separates the positive (humid) and the negative (dry) values. b) Precipitation reconstruction from the WA-PLS method. c) Temperature variation from Pollen PC2. The dashed line separates the positive (warm) and negative (cold) values. d) Temperature reconstruction from the WA-PLS method. The dashed lines of b and d are the absolute values estimated by the WA-PLS reconstruction and the continuous smooth line represent the mean values calculated by the LOESS modelling with a value of 0.2. Glacial-Interglacial F4-F5 pollen boundary (red line) and the boundary between MIS 12 and MIS 11 suggested by Lisiecki and Raymo (2005) (LR04)) is shown by the blue and beige boxes at ~424 ka. (For interpretation of the references to colour in this figure legend, the reader is referred to the web version of this article.)

Algae were very abundant with *Botryococcus* peaking slightly later than *Pediastrum*.

4.2.6. PZ-6 (between 422.3 ± 4.0 ka and 420.4 ± 3.7 ka; 97.14–97.05 m)

The forest was dominated by *Abies* (39.7–69.0 %), which further increased in this zone. The deciduous forest, represented by *Carpinus orientalis/Ostrya* (4.7–13 %), *Corylus* (1.3–6.7 %), *Ulmus* (1.3–5.0 %), and *Quercus* deciduous (0.7–5.7 %), was also an important component. Steppic taxa were almost absent (0.0–1.3 %).

Algae suffered a decrease compared with the previous PZ-5, but they were still abundant.

4.2.7. PZ-7 (between 420.4 ± 3.7 ka and 418.6 ± 3.6 ka; 97.05–96.95 m)

The *Abies* population remained domain in the forest (34.7–57.8 %), however, it experienced a decrease compared with PZ-6. The highest value of *Carpinus orientalis/Ostrya* was reached (3.7–18.3 %), followed in abundance by *Quercus* deciduous (3.7–9.0 %), *Carpinus betulus* (3.3–7.3 %), *Corylus* (1.7–6.3 %), and *Ulmus* (1.3–6.3 %). In this zone, *Botryococcus* (1.6–6.4 %) and *Pediastrum* (2.2–15.8 %) alternate.

4.3. Temperature and precipitation reconstructions

The mean annual precipitation and temperature reconstructions, with coefficients of determination (R^2) of 0.51 and 0.81, respectively, were obtained with the WA-PLS method (Fig. S3). The annual precipitation began to rise at 425.2 ± 4.6 ka from ~650 mm and peaked with a short interruption around 420.0 ± 3.6 ka, with estimated values near 1200 mm (Fig. 6). The same patterns are observed through time with pollen PC1 (interpreted as a variation in humidity; Fig. 4c), but with two main differences, (1) the peak observed by the PCA at 424.9 ± 4.4 ka is not that obvious in the quantitative precipitation reconstruction and (2) the peak at 426.9 ± 5.0 ka is overrepresented in the quantitative reconstruction, due to the low pollen concentration and the appearance of *Abies* in this sample. Both reconstructions are highly correlated with *Abies* population ($R_{PCA} = 0.98$; $R_{WA\text{-}PLS} = 0.91$), and *Alnus* ($R_{PCA} = 0.74$; $R_{WA\text{-}PLS} = 0.71$), *Carpinus* ($R_{PCA} = 0.87$; $R_{WA\text{-}PLS} = 0.80$) and *Corylus* ($R_{PCA} = 0.67$; $R_{WA\text{-}PLS} = 0.74$) association and inversely correlated with the steppe taxa ($R_{PCA} = -0.89$; $R_{WA\text{-}PLS} = -0.93$).

Several drawbacks of the temperature reconstructions could result in unreliable estimations. PC2 explains a very low variance value (8.9 %) of pollen data and the positive values correlate with the species forming the deciduous forests, although they do not show the same trend on the graphic representation. PC2 shows a distinct maximum at 424.2 ± 3.9 ka, which corresponds with the beginning of the interglacial. However, PC2 values decreased after this maximum, inferring temperatures similar to those of the glacial period during the rest of MIS 11c (Fig. 6). Regarding the WA-PLS temperature reconstruction, it exhibits a positive correlation with groups such as *Alnus* ($R_{WA\text{-}PLS} = 0.59$), *Corylus* ($R_{WA\text{-}PLS} = 0.66$), *Celtis* ($R_{WA\text{-}PLS} = 0.63$), and *Ulmus* ($R_{WA\text{-}PLS} = 0.46$), and a negative correlation with steppe ($R_{WA\text{-}PLS} = -0.59$) and herbaceous

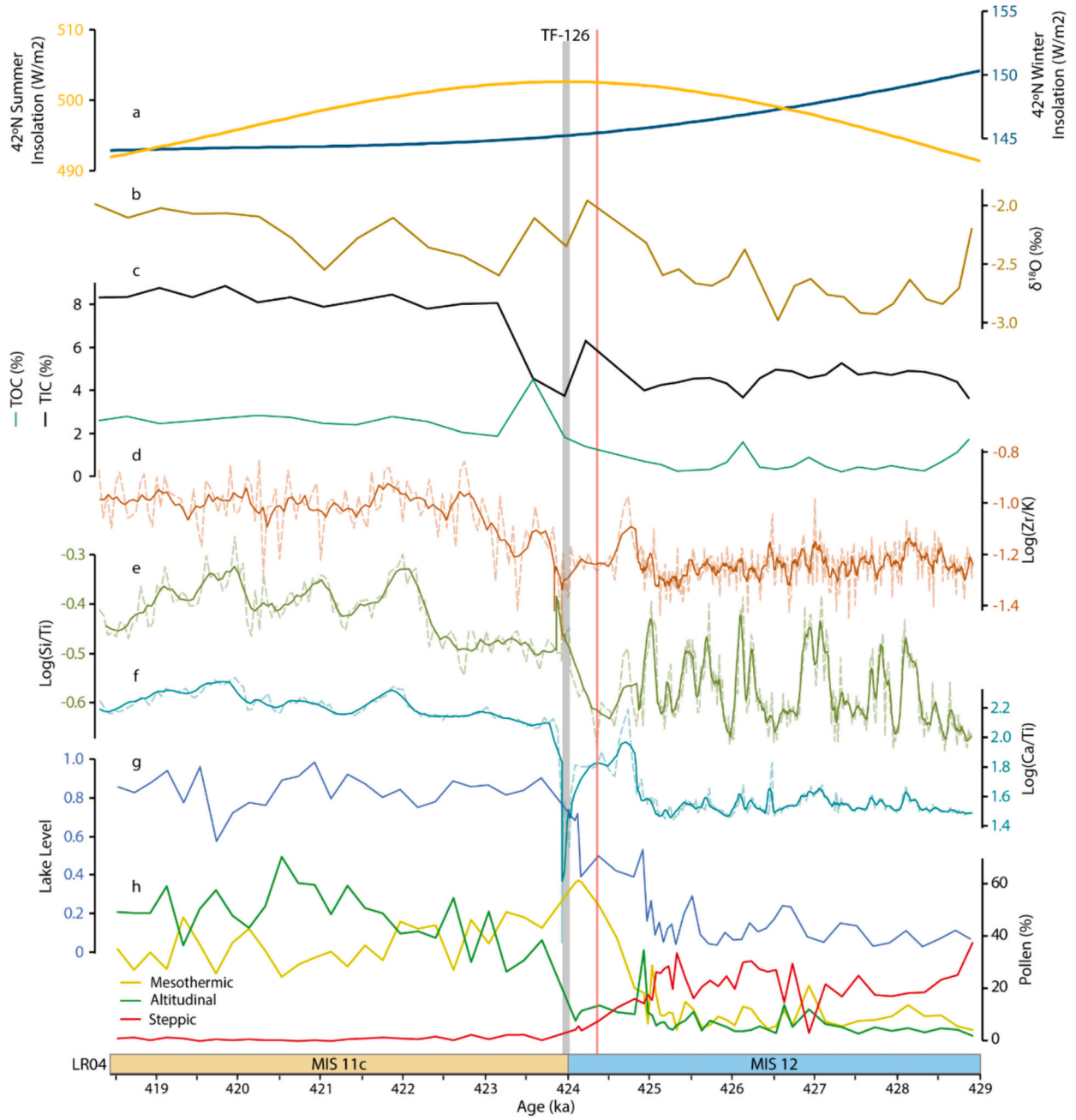

Fig. 7. Comparison of (a) summer and winter insolation at 42°N (Laskar et al., 2004) (b) δ18O from discrete samples, (c) Total Inorganic Carbon (TIC) (black) and Total Organic Carbon (TOC) (green) from discrete samples, (d) Zr/K, (e) Si/Ti, (f) Ca/Ti geochemical log-ratios from XRF scanning (dashed lines depict the actual values, while the continuous lines represent the mean average value for every 5 data points), (g) lake level according to Camuera et al. (2019) formula and (h) pollen associations percentages of the F5–58. Glacial-Interglacial F4-F5 pollen boundary is marked by the red line and the boundary between MIS 12 and MIS 11 suggested by Lisiecki and Raymo (2005) (LR04) is shown by the blue and beige boxes at ~424 ka. The TF-126 is indicated by the light-grey box. (For interpretation of the references to colour in this figure legend, the reader is referred to the web version of this article.)

groups. Moreover, the low concentration of pollen during MIS 12 (~429–425 ka; Fig. 3a) hampers reliable quantitative reconstruction. After the onset of the interglacial period, WA-PLS reconstructed temperatures show an opposite trend compared with the precipitation. A first increase in temperatures occurred at around 425.4 ± 4.9 ka from a mean estimated value of ~10 °C to a maximum of ~13 °C at 420.7 ± 3.6 ka, but the mean values decreased when estimated precipitation values increased (Fig. 6).

5. Discussion: climate and lake level reconstruction in the Fucino area

5.1. General remarks

The tephrochronologically independently dated high-resolution Fucino pollen record provides significant regional information about vegetation and climate variations during the interval 429.0 ± 5.0 ka to 418.5 ± 3.6 ka, encompassing the T-V (430.5 ± 1.5 ka to 426.0 ± 2.0 ka; Cheng et al., 2016) and the MIS 12-MIS 11 boundary (424.0 ± 4.0 ka; Lisiecki and Raymo, 2005) and the early stage of the MIS 11c

interglacial. At present, the Fucino basin (with an altitude of 650–680 m a.s.l.) is located in an area dominated by grasslands and deciduous forest with old-growth beech forest near the timberline and some conifer patches isolated at higher altitudes. Currently, the Fucino Basin is subjected to intense anthropogenic activity, particularly agriculture, which has significantly altered the composition of the natural/potential vegetation.

Previous studies (e.g. Joannin et al., 2011; Bertini et al., 2015; Camuera et al., 2019) have demonstrated that the abundance of temperate forest taxa serves as a valuable indicator of temperature and precipitation changes over time. In our study, we utilised deciduous and temperate-adapted forest species, such as *Quercus*, *Ulmus*, *Acer*, *Corylus*, and *Pterocarya*, as proxies for temperature (Fig. 4a) (e.g. Joannin et al., 2008). Notably, *Quercus* species have proven to be excellent proxies for distinguishing warm-humid from cold-arid paleoclimate phases (e.g. Denk et al., 2001; Joannin et al., 2008). *Abies* can also serve as proxy for precipitation and humidity (Alba-Sánchez et al., 2010), although disentangling temperature from precipitation signals can be challenging for certain species (Fig. S4). Previous palynological investigations indicate that increases in *Abies* abundance typically occur after the thermal maximum of interglacial periods and during a post-temperate phase, often associated with decreased summer insolation resulting in cooler conditions within overall still humid conditions (e.g. Tzedakis, 2007). Additionally, the abundance of herbaceous and steppic xerophytic plants (such as *Artemisia*, *Ephedra*, *Hippophäe*, and Amaranthaceae) can be utilised as indicators of cold and arid conditions (e.g. Fauquette et al., 1998; Tzedakis, 2007).

The XRF Ca values follow the same trend as the altitudinal taxa and estimated lake-level changes, whereas siliciclastic elements show variations similar to xerophytes (Figs. 7 and S2). The altitudinal taxa show some delay with respect to the Ca values, because Ca seems to be related with the lake productivity and the increase in the lake level. The lake productivity started to increase at the same time deduced by the rise in mesothermic taxa indicating the increase in temperature and, as consequence, enhanced eutrophication of the lake waters. At ~424.3 ± 4.0 ka, the altitudinal taxa indicate an increase in precipitation, which is also shown in the quantitative precipitation reconstruction (Figs. 6 and 7).

The abundance of algae (*Botryococcus, Pediastrum, Spirogyra, Zygnema*) is conditioned by lake level and shore surface area (Jiménez-Moreno et al., 2023), providing information about lake depth, availability of nutrients in the lake, and productivity. *Pediastrum* is a colonial green alga that indicates, for example, deeper lake water conditions (Fig. 4b and f; Nielsen and Sørensen, 1992; Anderson et al., 2020; Jiménez-Moreno et al., 2023) or eutrophication of the lake waters (Xiang et al., 2021). *Botryococcus* is a colonial green microalga growing in shallower water but is also affected by nutrient conditions (Fig. 4b and e; Guy-Ohlson, 1992; Jiménez-Moreno et al., 2023). The Log(Si/Ti) and Log(Ca/Ti) help to corroborate the productivity data provided by the algae community, as they are mostly the product of the activity and abundance of siliceous algae and calcite precipitation in the lake related to water temperatures, nutrient availability, and lake productivity, showing similar variations through time. During the dry and cold glacial MIS 12, the algae abundance was very low (Fig. 4). With the beginning of the interglacial period, the occurrence of algae increased, which matches with increasing TOC and TIC values, representing organic matter and authigenic calcite precipitation due to increasing lake productivity and temperatures. Strong variations in *Pediastrum* and *Botryococcus* values may indicate lake-level fluctuations, which are probably relatively low in magnitude (few meters only) but have a distinct impact on algae occurrences and nutrient conditions.

5.2. MIS 12 glaciation, T-V and beginning of MIS 11c (PZ-1 – PZ-5)

The full MIS 12 glacial condition are documented in Fucino F4-F5 sediment core between 429.0 ± 5.0 ka to 427.0 ± 5.0 ka, when vegetation was dominated by xerophytic and herbaceous taxa and *Pinus*, indicating cold and dry climate conditions, as confirmed by the steppic taxa association (Figs. 4a and 5). The mean temperature value reconstructed for this period in Fucino Basin was less than 10 °C with a mean annual precipitation between 600 and 700 mm (Fig. 6). The Fucino estimated temperature and precipitation values show similar trends compared to Lake Ohrid mean annual temperature and precipitation (Kousis et al., 2018) and Tenaghi Philippon mean annual air temperature (Ardenghi et al., 2019), being the Lake Ohrid the coldest reconstruction because of its slightly higher altitude and continentality (Fig. 9).

Throughout the glacial period, the lake level and lake productivity were at a minimum (Fig. 7). Low Log(Zr/K) and siliciclastic elements during this period (Figs. 7 and S2) indicate restricted erosion of fine-grained materials and inflow into the lake, which matches with high abundances of steppic taxa and implies moderate to low precipitation.

The transition from MIS 12 to MIS 11c, involved an increase in global temperatures as summer insolation levels raised (Laskar et al., 2004; Bouchet et al., 2023). This rapid climatic shift drove one of the biggest increases in global biosphere productivity (Brandon et al., 2020), changing dramatically the terrestrial vegetation cover, leading to the replacement of the steppic landscape by a dominant forest all along the Mediterranean region. This can be observed in the pollen data from the Iberian Margin (Hes et al., 2022), Alboran Sea (Sassoon et al., 2023), Lake Ohrid (Kousis et al., 2018) and Tenaghi Philippon (Koutsodendris et al., 2023a) (Figs. 8 and 9).

At Fucino, a humid event (PZ-2) occurred between 427.0 ± 5.0 ka and 426.6 ± 5.0 ka, indicated by a tree forest increase and steppic taxa decrease (Fig. 5). Also, the Log(Si/Ti) and Log(Ca/Ti) values increased, indicating higher temperatures and more rainfall. The peaks would correspond with an increase in lake productivity (more algae) and calcite precipitation triggered by warmer temperatures, more nutrients and more Ca ion supply for the catchment (e.g. Wagner et al., 2019). This humid event seems also to have occurred in the Alboran sea pollen record and is shown by an increase in altitudinal taxa and a slight reduction of steppic taxa (Sassoon et al., 2023) and at Lake Ohrid (Kousis et al., 2018; Koutsodendris et al., 2019; Donders et al., 2021) (Fig. 8), and could point to a wider regional climatic event. Following this event, the *Olea* percentage increased. This species is associated with warmer conditions, but in our study, it appears at the end of the glacial period, which could be the result of reworking and their percentage exaggeration due to low pollen concentration. Other mesothermic taxa increased during this event, but mostly due to enhanced humidity (Figs. 6 and S2). This is interpreted from the composition of the vegetation, mainly composed of deciduous taxa, with greater needs for water. Therefore, this record confirms the importance of relative humidity (precipitation versus evapotranspiration) in shaping the vegetation in the Mediterranean region, where climate is primarily influenced by temporal and seasonal precipitation variability (Ilvonen et al., 2022). The minimum temperature value reconstructed may correspond to the highest percentage of *Pinus* (*Pinus* total) during this zone (according to EMPDv2; Davis et al., 2020), which occurs in areas with mean annual temperatures below 10 °C (Fig. S4). These cold conditions may have influenced the relationship between evapotranspiration and precipitation, favouring the increase in humidity. The Log(Zr/K) value increases during this time as well as those "warm" pollen occurrences in the record, indicating an increase in erosion (Fig. 7), which agrees with the high precipitation values estimated from the quantitative reconstruction (Figs. 6 and 9).

The steppe taxa resume their dominance in the area following this event ending at 426.8 ± 5.0 ka, indicating further cold and arid conditions during the end of T-V (Fig. 5). Analysing the variation of xerophytic taxa during the end of the glacial period, some variability can be elucidated, with a slightly warmer and wetter period between two colder periods (with higher values of steppic taxa) following a "W" pattern characteristic of the Heinrich type events (Ht) (Singh et al.,

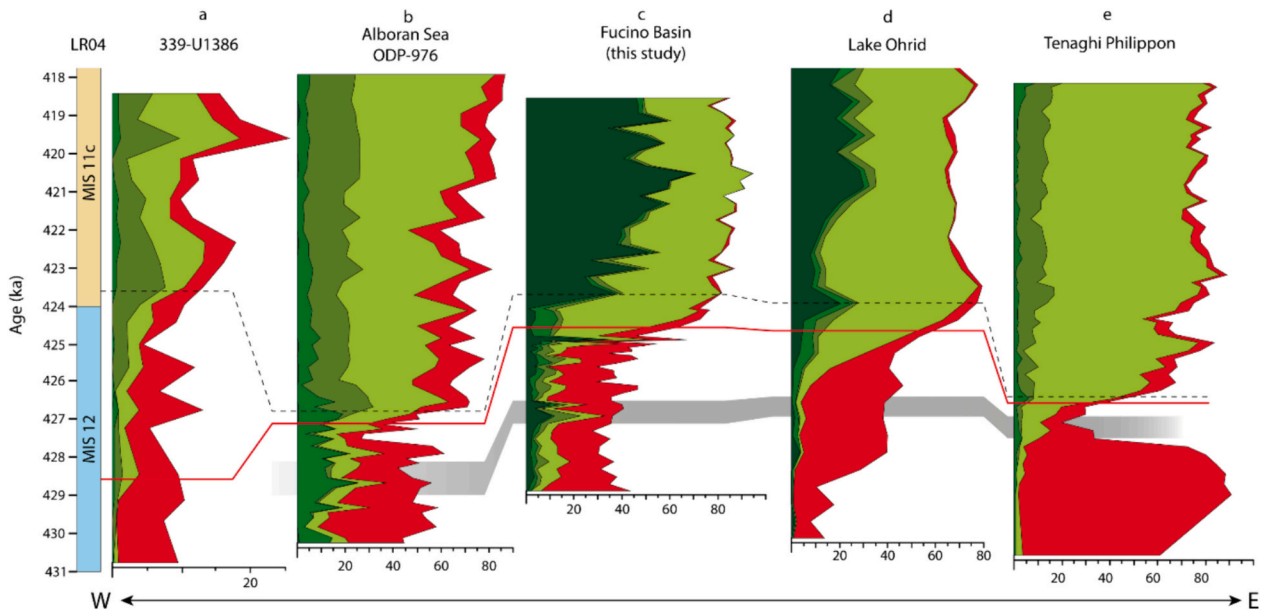

Fig. 8. Comparison of pollen records from (a) Iberian Margin (U1386 site; Hes et al., 2022), (b) Alboran Sea (ODP-976 site; Sassoon et al., 2023), (c) Fucino Basin (F4-F5 record; this study), (d) Lake Ohrid (Kousis et al., 2018; Koutsodendris, 2020), and (e) Tenaghi Philippon (Koutsodendris et al., 2023a, 2023b). Dark-green: Abies population; Green: altitudinal taxa; Brownish-green: Mediterranean taxa; Yellow-green: mesothermic taxa; Red: steppic taxa. The red line indicates the MIS 12–11c limit defined by their respective studies. The grey box correlates the PZ-2 defined in Fucino Basin. The dashed line correlates the beginning of the altitudinal taxa increase (for the continental eastern records) and the beginning of the Mediterranean taxa increase (for the marine western records). (For interpretation of the references to colour in this figure legend, the reader is referred to the web version of this article.)

2023). This Ht could correspond with the Ht4 identified by Rodrigues et al. (2011) at Iberian Margin with low Sea Surface Temperature (SST) values registered for this time (Fig. 9). The Ht are associated with SST cooling and reduction in Atlantic Meridional Overturning Circulation (AMOC), favouring the southward displacement of the Polar Front to the mid-latitudes of the North Atlantic (López-Martínez et al., 2006; Rodrigues et al., 2011, 2017; Singh et al., 2023) and they are associated within the beginning of terminations stages (e.g. Cheng et al., 2009). However, it is unclear if these terminal Ht are 'required' to start a termination, or if they are the result of the deglacial collapse of glacial ice sheets, and as such, consequences rather than causes of the glacial–interglacial changes (Hodell et al., 2008; Vázquez Riveiros et al., 2013). The Ht4 was the most extreme cold event registered in the SST at the Iberian Margin (Rodrigues et al., 2011), indicating the beginning of the T-V. This event has also been identified in the North Atlantic (Naafs et al., 2014), showing that it is of global importance (Hodell et al., 2008). We observe those temperature-humidity changes in the pollen record being able to define the duration of T-V just after the PZ-2 until the initial part of the PZ-4 (Figs. 3 and 5) for the Fucino pollen record.

After the T-V there was an initial succession when the steppe percentage began to decrease, a peak of mesothermic taxa was reached at 425.0 ± 4.5 ka, followed by a peak of altitudinal taxa (primarily *Abies*; Fig. 5). With a higher amplitude, the same transition can be observed between 424.2 ± 3.9 ka and 420.6 ± 3.9 ka, with mesothermic vegetation increasing and reaching a peak related to the increase and maxima in summer insolation (Fig. 7), the xerophytes then reached their minimum, and finally, the mesothermic vegetation was replaced by altitudinal taxa, which became dominant. The duration of the warmer period could be evidenced by the pollen PC2 maxima but is not reliable in intensity (Figs. 4d and 6c). The increase in the Log(Zr/K) indicates sedimentation of coarser material, which means a higher transport energy, probably related to more rainfall and higher activity of the inlet streams. This detrital influx increased in a opposite pattern compared to xerophytes, whereas the lake level and its productivity (Log(Ca/Ti), Log (Si/Ti) and NPP PC1) increased abruptly (Figs. 4e and 7).

During this climatic transition, the mesothermic taxa occurring at Fucino were mainly composed by *Quercus* deciduous, *Ulmus*, *Acer,* and *Tilia,* which are more related to warmer and more humid conditions than the previous steppic taxa. Subsequently, those deciduous taxa were replaced by *Carpinus*, *Carpinus orientalis/Ostrya*, *Corylus*, *Celtis* and *Alnus*, which are related to more humid conditions (according to the PCA) (Fig. 4a) (Denk et al., 2001). A similar substitution of the deciduous taxa occurred in Lake Kopais (Southeeast Greece; Okuda et al., 2001) and at Lake Ohrid (Kousis et al., 2018). This confirms the typical G/I cycle described by Tzedakis (2007) and Jiménez-Moreno et al. (2013), where the transition period into the interglacial is warmer and drier, followed by a more humid forest in the temperate phase of the interglacial. Lake Ohrid seems to exhibit a more similar vegetation evolution to Fucino than to other Mediterranean records, with a similar beginning of the T-V with the decline of the steppic taxa and their replacement by mesothermic taxa (Fig. 8). The quantitative reconstructions for this transition estimated an increase in precipitation values, corroborating the wetter climate for Fucino Basin and Lake Ohrid than other Mediterranean pollen records, such as Tenaghi Philippon and Alboran Sea, where the altitudinal taxa did not have enough representation. The rise in Fucino lake's level, the increase in humidity and great abundance of altitudinal taxa may have been caused by the deglaciation of the mountain glaciers around the Fucino basin (Cheddadi et al., 2005; Giaccio et al., 2019). The comparison of the mean annual temperatures estimations with other Mediterranean records shows that Lake Ohrid temperatures were lower than at Fucino during the glacial period, but after the T-V both regions reached similar temperature values (Fig. 9).

5.3. MIS 11c (PZ-6, PZ-7)

Compared with other paleoclimatic estimations following the T-V, such as the SST from Iberian Margin (Rodrigues et al., 2011) or North Atlantic SST (Naafs et al., 2014), where temperatures increased from ~13 °C to ~17 °C (Fig. 9) relatively abruptly the estimated temperatures in the Fucino Basin continental record increased more gradually from ~9.5 °C to a maximum of 13.0 °C (Fig. 6). Estimated temperatures in

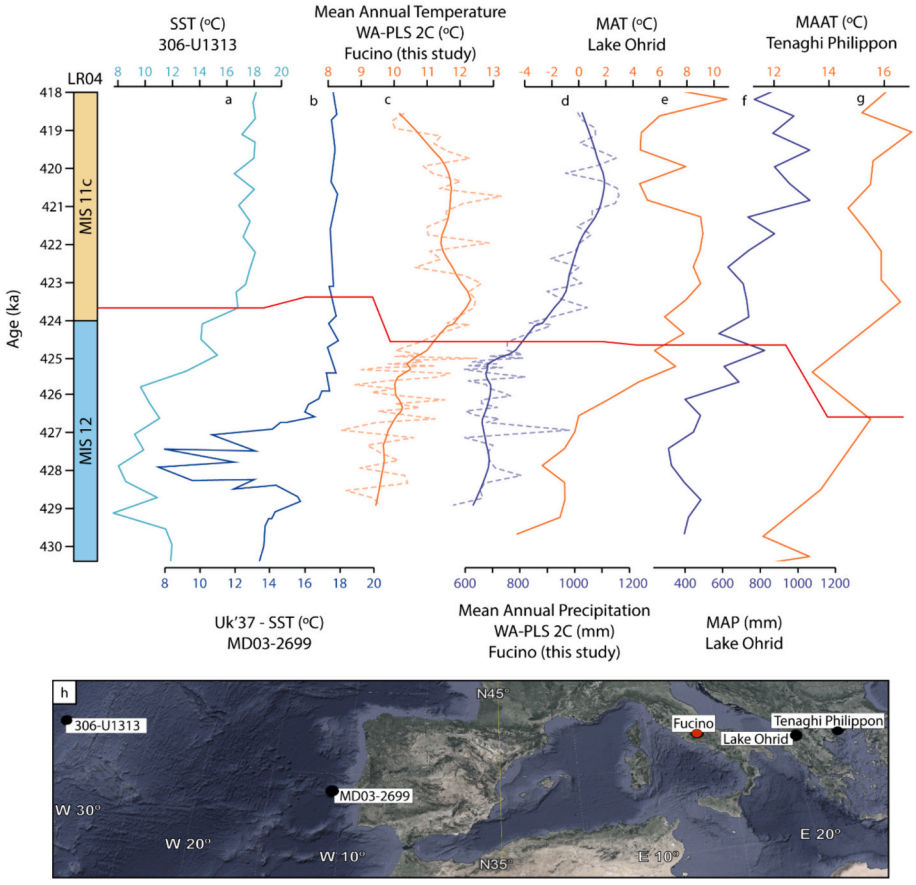

Fig. 9. Comparison of quantitative reconstructions of Sea Surface Temperature (SST) and continental temperatures and precipitation. a) North Atlantic SST from a alkenone based reconstruction (Naafs et al., 2013, 2014). b) Iberian margin SST from alkenones ($U^{k'}_{37}$ index) (Rodrigues et al., 2011). c) Mean Annual Temperature from Fucino Basin using the WA-PLS method from pollen data (Fig. 6; this study). d) Mean Annual Precipitation from Fucino Basin using the Weighted-Averaging Partial-Least Squares (WA-PLS) method from pollen data (Fig. 6; this study). e) Lake Ohrid Mean Annual Temperature (MAT) using the Modern Analogue Technique from pollen data (Koutsodendris, 2020). f) Lake Ohrid Mean Annual Precipitation (MAP) using the Modern Analogue Technique from pollen data (Koutsodendris, 2020). g) Tenaghi Mean Annual Air Temperature (MAAT) calculated by GDGTs (Ardenghi et al., 2019). h) Location of the sites. The red line marks the MIS 12-MIS 11c boundary defined in the different studies. (For interpretation of the references to colour in this figure legend, the reader is referred to the web version of this article.)

Lake Ohrid (Kousis et al., 2018) increased from ~1.5 °C to a 10 °C at around 423 ka (Fig. 9), showing a more drastic change in temperatures during this time. The temperatures reconstructed from Tenaghi Philippon (Ardenghi et al., 2019) did not experience such an abrupt change, depicting a temperature difference from the beginning to the end of T-V of ~2.5 °C, a temperature range similar to the Fucino Basin reconstructions. Precipitation during MIS 11c in Fucino Basin increased gradually reaching annual values near 1200 mm at around 421.0 ± 4.2 ka (Fig. 6). This increase in precipitation to similar values is also observed in Sulmona Basin (Italy; Regattieri et al., 2016). It could be explained by the orographic effect, reaching higher precipitation values at the summit areas of the mountains drainage basins (Regattieri et al., 2016). The records form Fucino Basin and Lake Ohrid also indicate similar estimated precipitation patterns (Fig. 9), with MIS 11c being one of the highest estimated values recorded in Lake Ohrid over the last 800 ka (Wagner et al., 2019). An increase in the pollen concentration, with *Abies* being the dominant pollen taxon, occurred during this interglacial (e.g. Brandon et al., 2020), coupled with an elevated sedimentation rate and diminished terrigenous input.

The altitudinal taxa during MIS 11c in Fucino Basin exhibit a consistent increase, culminating in a peak of *Abies* of about 69 % at 420.5 ± 3.8 ka. This trend follows, with some delay due to the vegetation response to the external climatic parameters, the summer insolation through time (Fig. 7) and can also be observed at Lake Ohrid (Fig. 8). *Abies* populations are in general restricted to moist mountainous habitats (Alba-Sánchez et al., 2010), but such a high percentage of *Abies* has never been observed previously in other pollen records from in Europe during an interglacial. The increase of *Abies* at the beginning of the interglacial is less than 20 % and 30 % at Tenaghi Philippon (Pross et al., 2015) and at Lake Ohrid (Kousis et al., 2018) respectively, as *Abies* pollen grains cannot be transported for long distances by the wind due to their large pollen size, and hence their occurrence in the fossil record indicates proximity to the pollen source (Erdtman, 1969; Moreno-Amat et al., 2017). This means that *Abies* constituted the main forest species up to high altitudes in Fucino Basin during the MIS 11c interglacial. Previous studies on the present-day *Abies* ecology show that *Abies* growing at lower elevations has a much broader ecological amplitude (including pioneer characteristics and drought tolerance) than those growing at higher elevations (Dobrowolska, 1998; Burga and Hussendörfer, 2001; Schmidl et al., 2005; Kozáková et al., 2011), which could explain why *Abies* is so abundant in the Fucino Basin during the MIS 11c interglacial. However, *Abies* is less abundant in other records, which could indicate that the abundance is strongly influenced by the local orography and less by precipitation.

The comparison of the central Mediterranean pollen records shows an abrupt increase of Mediterranean taxa just after the T-V, which is only marginally represented at Fucino Basin and Lake Ohrid (Fig. 8). We can conclude from this observation that the Mediterranean region experienced an increase in temperatures and an abrupt change in vegetation during the G/I transition, but the central longitudinal

Mediterranean area was more influenced by the balance of precipitation and evapotranspiration, with high precipitation values at that time (Figs. 8 and 9).

6. Conclusions

The palynological record from the Fucino F4-F5 sediment core interval, independently dated between 429.0 ± 5.0 ka to 418.5 ± 3.6 ka, permitted us to reconstruct vegetation and environmental over the late MIS 12 glacial, the glacial Termination V (T-V), and the early MIS 11c interglacial, one of the major changes of Quaternary Earth's climatic system history.

The MIS 12 in Fucino Basin was characterised by a very dry and cold climate evidenced by the abundant steppic taxa.

Centennial-scale variability seems to characterise the Fucino pollen record in glacial MIS 12, with Heinrich-type events identified withing the course of the T-V and highly variable mean-annual temperature and precipitations, which were 10.0–9.5 °C and 700–650 mm, in average. In comparison with other Mediterranean pollen records, this reveals a large regional variability.

A relative humid event occurred between 427.0 ± 5.0 ka and 426.6 ± 5.0 ka and led, to a decrease in steppic taxa and an increase in tree forest from less than 20 % to almost 90 %, despite minimal astronomical forcing.

The onset of warmest, interglacial conditions at Fucino, demarcated by the increase in mesothermic taxa, is independently-dated to 424.5 ± 4.0 ka, which corresponds with the MIS 12/11 transition at 424 ± 4.0 ka in the benthic $\delta^{18}O$ record.

During the MIS 11c interglacial, the mean-annual temperatures and precipitations were lesser variable, compared with MIS 12 glacial period. The temperatures reached their maximum of ~12.5 °C during the early stage of the MIS 11c interglacial at 423.5 ± 3.8 ka, to then gradually decreased to ~10.0 °C at 418.5 ± 3.6 ka, while precipitations increased more gradually from ~800 mm/yr at the very beginning of the MIS 11c to a maximum of 1200 mm/yr at 421.0 ± 4.2 ka.

Overall, during the studied interval, the observed variability of the vegetation of the Mediterranean region was mainly controlled by a change in the hydrological regime and balance, which, in turn, was led by oceanic-atmospheric and precipitation/evaporation dynamics, despite minimal astronomical forcing.

Author contributions

P. Vera-Polo performed the pollen analysis, pollen data interpretation and wrote the paper. G. Jiménez-Moreno and L. Sadori supervised all the process about conceptualisation and interpretations of the pollen data. B. Giaccio and G. Zanchetta retrieved the sedimentary record and worked on the chronological control of the core. All authors contributed to the interpretation, discussed the results and provided inputs to the paper.

CRediT authorship contribution statement

Pablo Vera-Polo: Writing – original draft, Visualization, Resources, Project administration, Methodology, Investigation, Formal analysis, Data curation, Conceptualization. **Laura Sadori:** Writing – review & editing, Supervision, Funding acquisition, Conceptualization. **Gonzalo Jiménez-Moreno:** Writing – review & editing, Validation, Supervision, Funding acquisition, Conceptualization. **Alessia Masi:** Writing – review & editing. **Biagio Giaccio:** Writing – review & editing, Visualization, Resources, Funding acquisition, Data curation. **Giovanni Zanchetta:** Writing – review & editing, Data curation. **P. Chronis Tzedakis:** Writing – review & editing. **Bernd Wagner:** Writing – review & editing.

Declaration of competing interest

The authors declare that they have no known competing financial interests or personal relationships that could have appeared to influence the work reported in this paper.

Data availability

Data will be made available on request.

Acknowledgements

This article is a contribution of the project "CLImate Change: the study of past interglacials from Mediterranean pollen records to understand our future (CLIC)" supported by the Italian University of La Sapienza. We thank the project "FUcino Tephrochronology Unites Quaternary REcords (FUTURE)" for recollecting the geochemical and tephrocronological data. This work is the result of an international consortium between University of Granada, University of Rome "La Sapienza", National and Kapodistrian University of Athens, IGAG-CNR, University of Pisa, University College London and University of Cologne. Also thank for the PhD scolarship "Dottorati PON" (Ministero dell'Università e della Ricerca) for the financial support of the PhD (Grant number: DOT 11094 CUP B89J21024760001). GJM acknowledges funding from PID2021-125619OB-C21 by the Ministerio de Ciencia e Innovación of Spain, the Agencia Estatal de Investigación and the Fondo Europeo de Desarrollo Regional FEDER MCIN/AEI/10.13039/501100011033/FEDER, UE.

Appendix A. Supplementary data

Supplementary data to this article can be found online at https://doi.org/10.1016/j.palaeo.2024.112486.

References

Alba-Sánchez, F., López-Sáez, J.A., Pando, B.B., Linares, J.C., Nieto-Lugilde, D., López-Merino, L., 2010. Past and present potential distribution of the Iberian Abies species: a phytogeographic approach using fossil pollen data and species distribution models. Divers. Distrib. 16, 214–228. https://doi.org/10.1111/j.1472-4642.2010.00636.x.

Allen, J.R.M., Watts, W.A., Huntley, B., 2000. Weichselian palynostratigraphy, palaeovegetation and palaeoenvironment; the record from Lago Grande di Monticchio, southern Italy. Quat. Int. 73–74, 91–110. https://doi.org/10.1016/S1040-6182(00)00067-7.

Altolaguirre, Y., Bruch, A.A., Gibert, L., 2020. A long Early Pleistocene pollen record from Baza Basin (SE Spain): major contributions to the palaeoclimate and palaeovegetation of Southern Europe. Quat. Sci. Rev. 231, 106199 https://doi.org/10.1016/j.quascirev.2020.106199.

Anderson, R.S., Jiménez-Moreno, G., Belanger, M., Briles, C., 2020. Fire history of the unique high-elevation Snowmastodon (Ziegler Reservoir) site during MIS 6–4, with comparisons of TII to TI in the southern Colorado Rockies. Quat. Sci. Rev. 232, 106213 https://doi.org/10.1016/j.quascirev.2020.106213.

Ardenghi, N., Mulch, A., Koutsodendris, A., Pross, J., Kahmen, A., Niedermeyer, E.M., 2019. Temperature and moisture variability in the eastern Mediterranean region during Marine Isotope Stages 11–10 based on biomarker analysis of the Tenaghi Philippon peat deposit. Quat. Sci. Rev. 225, 105977. https://doi.org/10.1016/j.quascirev.2019.105977.

Bakker, P., Clark, P.U., Golledge, N.R., Schmittner, A., Weber, M.E., 2017. Centennial-scale Holocene climate variations amplified by Antarctic ice sheet discharge. Nature 541, 72–76. https://doi.org/10.1038/nature20582.

Barker, S., Chen, J., Gong, X., Jonkers, L., Knorr, G., Thornalley, D., 2015. Icebergs not the trigger for North Atlantic cold events. Nature 520, 333–336. https://doi.org/10.1038/nature14330.

Bennett, K.D., Tzedakis, P.C., Willis, K.J., 1991. Quaternary refugia of north European trees. J. Biogeogr. 18, 103–115. https://doi.org/10.2307/2845248.

Berger, W., Wefer, G., 2003. On the dynamics of the ice ages: stage-11 paradox, Mid-Brunhes climate shift, and 100-Ky cycle. In: Wash. DC Am Geophys. Union Geophys. Monogr. Ser, 137, pp. 41–59. https://doi.org/10.1029/137GM04.

Bertini, A., Toti, F., Marino, M., Ciaranfi, N., 2015. Vegetation and climate across the Early–Middle Pleistocene transition at Montalbano Jonico, southern Italy. In: Quat. Int., The Quaternary System and its Formal Subdivision, 383, pp. 74–88. https://doi.org/10.1016/j.quaint.2015.01.003.

Blaauw, M., Christen, J.A., 2011. Flexible paleoclimate age-depth models using an autoregressive gamma process. Bayesian Anal. 6, 457–474. https://doi.org/10.1214/11-BA618.

Blasi, C., Del Vico, E., 2012. High mountain vegetation of the Apennines. In: Rintelner Symp. X, 24, pp. 179–194.
Blasi, C., Biondi, E., Poldini, L., Sburlino, G., Venanzoni, R., Rosati, L., Gigante, D., Anzellotti, I., Bonacquisti, S., Del Vico, E., Di Marzio, P., Mollo, B., Tilia, A., 2010. La vegetazione d'Italia, Carta delle Serie di Vegetazione. Scala 1:500.000. Palombi & Partner Roma.
Blasi, C., Capotorti, G., Alós Ortí, M.M., Anzellotti, I., Attorre, F., Azzella, M.M., Carli, E., Copiz, R., Garfì, V., Manes, F., Marando, F., Marchetti, M., Mollo, B., Zavattero, L., 2017. Ecosystem mapping for the implementation of the European biodiversity strategy at the national level: the case of Italy. Environ. Sci. Policy 78, 173–184. https://doi.org/10.1016/j.envsci.2017.09.002.
Bouchet, M., Landais, A., Grisart, A., Parrenin, F., Prié, F., Jacob, R., Fourré, E., Capron, E., Raynaud, D., Lipenkov, V.Y., Loutre, M.-F., Extier, T., Svensson, A., Legrain, E., Martinerie, P., Leuenberger, M., Jiang, W., Ritterbusch, F., Lu, Z.-T., Yang, G.-M., 2023. The AICC2023 chronological framework and associated timescale for the EPICA Dome C ice core. In: Ice Dynamics/Ice Cores/Milankovitch. https://doi.org/10.5194/egusphere-2023-1081.
Brandon, M., Landais, A., Duchamp-Alphonse, S., Favre, V., Schmitz, L., Abrial, H., Prié, F., Extier, T., Blunier, T., 2020. Exceptionally high biosphere productivity at the beginning of marine isotopic stage 11. Nat. Commun. 11, 2112. https://doi.org/10.1038/s41467-020-15739-2.
Brown, E.T., 2011. Lake Malawi's response to "megadrought" terminations: sedimentary records of flooding, weathering and erosion. In: Palaeogeogr. Palaeoclimatol. Palaeoecol., Southern Hemisphere Tropical Climate Over the Past 145ka: Results of the Lake Malawi Scientific Drilling Project, East Africa, 303, pp. 120–125. https://doi.org/10.1016/j.palaeo.2010.01.038.
Burga, C.A., Hussendörfer, E., 2001. Vegetation history of *Abies alba* Mill. (silver fir) in Switzerland – pollen analytical and genetic surveys related to aspects of vegetation history of *Picea abies* (L.) H. Karsten (Norway spruce). Veg. Hist. Archaeobotany 10, 151–159. https://doi.org/10.1007/PL00006927.
Caielli, G., Maffucci, R., de Franco, R., Bigi, S., Parotto, M., Mollica, R., Gaudiosi, I., Simionato, M., Romanelli, M., De Marchi, N., Cavinato, G.P., 2023. Fucino Basin structure revealed by the tomography and the reusing of the CROP11 seismic data. Tectonophysics 865, 230043. https://doi.org/10.1016/j.tecto.2023.230043.
Camuera, J., Jiménez-Moreno, G., Ramos-Román, M.J., García-Alix, A., Toney, J.L., Anderson, R.S., Jiménez-Espejo, F., Bright, J., Webster, C., Yanes, Y., Carrión, J.S., 2019. Vegetation and climate changes during the last two glacial-interglacial cycles in the western Mediterranean: a new long pollen record from Padul (southern Iberian Peninsula). Quat. Sci. Rev. 205, 86–105. https://doi.org/10.1016/j.quascirev.2018.12.013.
Camuera, J., Ramos-Román, M.J., Jiménez-Moreno, G., García-Alix, A., Ilvonen, L., Ruha, L., Gil-Romera, G., González-Sampériz, P., Seppä, H., 2022. Past 200 kyr hydroclimate variability in the western Mediterranean and its connection to the African humid periods. Sci. Rep. 12, 9050. https://doi.org/10.1038/s41598-022-12047-1.
Cavinato, G.P., Carusi, C., Dall'Asta, M., Miccadei, E., Piacentini, T., 2002. Sedimentary and tectonic evolution of Plio–Pleistocene alluvial and lacustrine deposits of Fucino Basin (central Italy). Sediment. Geol. 148, 29–59. https://doi.org/10.1016/S0037-0738(01)00209-3.
Cheddadi, R., de Beaulieu, J.-L., Jouzel, J., Andrieu-Ponel, V., Laurent, J.-M., Reille, M., Raynaud, D., Bar-Hen, A., 2005. Similarity of vegetation dynamics during interglacial periods. Proc. Natl. Acad. Sci. 102, 13939–13943. https://doi.org/10.1073/pnas.0501752102.
Cheng, H., Edwards, R.L., Broecker, W.S., Denton, G.H., Kong, X., Wang, Y., Zhang, R., Wang, X., 2009. Ice age terminations. Science 326, 248–252. https://doi.org/10.1126/science.1177840.
Cheng, H., Edwards, R.L., Sinha, A., Spötl, C., Yi, L., Chen, S., Kelly, M., Kathayat, G., Wang, X., Li, X., Kong, X., Wang, Y., Ning, Y., Zhang, H., 2016. The Asian monsoon over the past 640,000 years and ice age terminations. Nature 534, 640–646. https://doi.org/10.1038/nature18591.
Chevalier, M., Davis, B.A.S., Heiri, O., Seppä, H., Chase, B.M., Gajewski, K., Lacourse, T., Telford, R.J., Finsinger, W., Guiot, J., Kühl, N., Maezumi, S.Y., Tipton, J.R., Carter, V.A., Brussel, T., Phelps, L.N., Dawson, A., Zanon, M., Vallé, F., Nolan, C., Mauri, A., de Vernal, A., Izumi, K., Holmström, L., Marsicek, J., Goring, S., Sommer, P.S., Chaput, M., Kupriyanov, D., 2020. Pollen-based climate reconstruction techniques for late Quaternary studies. Earth Sci. Rev. 210, 103384 https://doi.org/10.1016/j.earscirev.2020.103384.
Croudace, I.W., Rothwell, R.G. (Eds.), 2015. Micro-XRF Studies of Sediment Cores: Applications of a Non-Destructive Tool for the Environmental Sciences, Developments in Paleoenvironmental Research. Springer Netherlands, Dordrecht. https://doi.org/10.1007/978-94-017-9849-5.
Cuven, S., Francus, P., Lamoureux, S., 2011. Mid to late Holocene hydroclimatic and geochemical records from the varved sediments of East Lake, Cape Bounty, Canadian High Arctic. Quat. Sci. Rev. 30, 2651–2665. https://doi.org/10.1016/j.quascirev.2011.05.019.
Davis, B.A.S., Chevalier, M., Sommer, P., Carter, V.A., Finsinger, W., Mauri, A., Phelps, L.N., Zanon, M., Abegglen, R., Åkesson, C.M., Alba-Sánchez, F., Anderson, R.S., Antipina, T.G., Atanassova, J.R., Beer, R., Belyanina, N.I., Blyakharchuk, T.A., Borisova, O.K., Bozilova, E., Bukreeva, G., Bunting, M.J., Clò, E., Colombaroli, D., Combourieu-Nebout, N., Desprat, S., Di Rita, F., Djamali, M., Edwards, K.J., Fall, P.L., Feurdean, A., Fletcher, W., Florenzano, A., Furlanetto, G., Gaceur, E., Galimov, A.T., Gałka, M., García-Moreiras, I., Giesecke, T., Grindean, R., Guido, M.A., Gvozdeva, I.G., Herzschuh, U., Hjelle, K.L., Ivanov, S., Jahns, S., Jankovska, V., Jiménez-Moreno, G., Karpińska-Kołaczek, M., Kitaba, I., Kołaczek, P., Lapteva, E.G., Latałowa, M., Lebreton, V., Leroy, S., Leydet, M., Lopatina, D.A., López-Sáez, J.A., Lotter, A.F., Magri, D., Marinova, E., Matthias, I., Mavridou, A., Mercuri, A.M., Mesa-Fernández, J.M., Mikishin, Y.A., Milecka, K., Montanari, C., Morales-Molino, C., Mrotzek, A., Muñoz Sobrino, C., Naidina, O.D., Nakagawa, T., Nielsen, A.B., Novenko, E.Y., Panajiotidis, S., Panova, N.K., Papadopoulou, M., Pardoe, H.S., Pędziszewska, A., Petrenko, T.I., Ramos-Román, M.J., Ravazzi, C., Rösch, M., Ryabogina, N., Sabariego Ruiz, S., Salonen, J.S., Sapelko, T.V., Schofield, J.E., Seppä, H., Shumilovskikh, L., Stivrins, N., Stojakowits, P., Svobodova Svitavska, H., Święta-Musznicka, J., Tantau, I., Tinner, W., Tobolski, K., Tonkov, S., Tsakiridou, M., Valsecchi, V., Zanina, O.G., Zimny, M., 2020. The Eurasian Modern Pollen Database (EMPD), version 2. Earth Syst. Sci. Data 12, 2423–2445. https://doi.org/10.5194/essd-12-2423-2020.
Denk, T., Frotzler, N., Davitashvili, N., 2001. Vegetational patterns and distribution of relict taxa in humid temperate forests and wetlands of Georgia (Transcaucasia). Biol. J. Linn. Soc. 72, 287–332. https://doi.org/10.1111/j.1095-8312.2001.tb01318.x.
Djamali, M., Cilleros, K., 2020. Statistically significant minimum pollen count in Quaternary pollen analysis; the case of pollen-rich lake sediments. Rev. Palaeobot. Palynol. 275, 104156 https://doi.org/10.1016/j.revpalbo.2019.104156.
Dobrowolska, D., 1998. Structure of silver fir (*Abies alba* Mill.) natural regeneration in the `Jata' reserve in Poland. For. Ecol. Manag. 110, 237–247. https://doi.org/10.1016/S0378-1127(98)00286-2.
Donders, T., Panagiotopoulos, K., Koutsodendris, A., Bertini, A., Mercuri, A.M., Masi, A., Combourieu-Nebout, N., Joannin, S., Kouli, K., Kousis, I., Peyron, O., Torri, P., Florenzano, A., Francke, A., Wagner, B., Sadori, L., 2021. 1.36 million years of Mediterranean forest refugium dynamics in response to glacial–interglacial cycle strength. Proc. Natl. Acad. Sci. 118, e2026111118 https://doi.org/10.1073/pnas.2026111118.
Ehlers, J., Gibbard, P., 2008. Extent and chronology of Quaternary glaciation. Episodes J. Int. Geosci. 31, 211–218. https://doi.org/10.18814/epiiugs/2008/v31i2/004.
Erdtman, G., 1969. Handbook of Palynology: Morphology, Taxonomy, Ecology. Ejnar Munksgaard.
Fauquette, S., Guiot, J., Suc, J.-P., 1998. A method for climatic reconstruction of the Mediterranean Pliocene using pollen data. Palaeogeogr. Palaeoclimatol. Palaeoecol. 144, 183–201. https://doi.org/10.1016/S0031-0182(98)00083-2.
Fick, S.E., Hijmans, R.J., 2017. WorldClim 2: new 1-km spatial resolution climate surfaces for global land areas. Int. J. Climatol. 37 (12), 4302–4315. https://doi.org/10.1002/joc.5086.
Frate, L., Carranza, M.L., Evangelista, A., Stinca, A., Schaminée, J.H.J., Stanisci, A., 2018. Climate and land use change impacts on Mediterranean high-mountain vegetation in the Apennines since the 1950s. Plant Ecol. Divers. 11, 85–96. https://doi.org/10.1080/17550874.2018.1473521.
Freytet, P., Verrecchia, E.P., 2002. Lacustrine and palustrine carbonate petrography: an overview. J. Paleolimnol. 27, 221–237. https://doi.org/10.1023/A:1014263722766.
Galadini, F., Galli, P., 2000. Active tectonics in the central Apennines (Italy) – input data for seismic hazard assessment. Nat. Hazards 22, 225–268. https://doi.org/10.1023/A:1008149531980.
Galadini, F., Messina, P., 2004. Early–Middle Pleistocene eastward migration of the Abruzzi Apennine (central Italy) extensional domain. J. Geodyn. 37, 57–81. https://doi.org/10.1016/j.jog.2003.10.002.
Giaccio, B., Regattieri, E., Zanchetta, G., Wagner, B., Galli, P., Mannella, G., Niespolo, E., Peronace, E., Renne, P.R., Nomade, S., Cavinato, G.P., Messina, P., Sposato, A., Boschi, C., Florindo, F., Marra, F., Sadori, L., 2015. A key continental archive for the last 2 Ma of climatic history of the central Mediterranean region: a pilot drilling in the Fucino Basin, central Italy. Sci. Drill. 20, 13–19. https://doi.org/10.5194/sd-20-13-2015.
Giaccio, B., Niespolo, E.M., Pereira, A., Nomade, S., Renne, P.R., Albert, P.G., Arienzo, I., Regattieri, E., Wagner, B., Zanchetta, G., Gaeta, M., Galli, P., Mannella, G., Peronace, E., Sottili, G., Florindo, F., Leicher, N., Marra, F., Tomlinson, E.L., 2017. First integrated tephrochronological record for the last ~190 kyr from the Fucino Quaternary lacustrine succession, central Italy. Quat. Sci. Rev. 158, 211–234. https://doi.org/10.1016/j.quascirev.2017.01.004.
Giaccio, B., Leicher, N., Mannella, G., Monaco, L., Regattieri, E., Wagner, B., Zanchetta, G., Gaeta, M., Marra, F., Nomade, S., Palladino, D.M., Pereira, A., Scheidt, S., Sottili, G., Wonik, T., Wulf, S., Zeeden, C., Ariztegui, D., Cavinato, G.P., Dean, J.R., Florindo, F., Leng, M.J., Macrì, P., Niespolo, E., Renne, P.R., Rolf, C., Sadori, L., Thomas, C., Tzedakis, P.C., 2019. Extending the tephra and palaeoenvironmental record of the central Mediterranean back to 430 ka: a new core from Fucino Basin, central Italy. Quat. Sci. Rev. 225, 106003 https://doi.org/10.1016/j.quascirev.2019.106003.
Giaccio, B., Marino, G., Marra, F., Monaco, L., Pereira, A., Zanchetta, G., Gaeta, M., Leicher, N., Nomade, S., Palladino, D.M., Sottili, G., Guillou, H., Scao, V., 2021. Tephrochronological constraints on the timing and nature of sea-level change prior to and during glacial termination V. Quat. Sci. Rev. 263, 106976 https://doi.org/10.1016/j.quascirev.2021.106976.
Grimm, E.C., 1987. CONISS: a FORTRAN 77 program for stratigraphically constrained cluster analysis by the method of incremental sum of squares. Comput. Geosci. 13, 13–35. https://doi.org/10.1016/0098-3004(87)90022-7.
Guy-Ohlson, D., 1992. Botryococcus as an aid in the interpretation of palaeoenvironment and depositional processes. Rev. Palaeobot. Palynol. 71, 1–15. https://doi.org/10.1016/0034-6667(92)90155-A.
Hammer, O., Harper, D.A.T., Ryan, P.D., 2001. PAST: Paleontological Statistics Software Package for Education and Data Analysis.
Hays, J.D., Imbrie, J., Shackleton, N.J., 1976. Variations in the Earth's orbit: pacemaker of the ice ages: for 500,000 years, major climatic changes have followed variations in obliquity and precession. Science 194, 1121–1132. https://doi.org/10.1126/science.194.4270.1121.

Hes, G., Sánchez Goñi, M.F., Bouttes, N., 2022. Impact of terrestrial biosphere on the atmospheric CO2 concentration across termination V. Clim. Past 18, 1429–1451. https://doi.org/10.5194/cp-18-1429-2022.

Hodell, D.A., Channell, J.E.T., Curtis, J.H., Romero, O.E., Röhl, U., 2008. Onset of "Hudson Strait" Heinrich events in the eastern North Atlantic at the end of the middle Pleistocene transition (~640 ka)? Paleoceanography 23. https://doi.org/10.1029/2008PA001591.

Ilvonen, L., López-Sáez, J.A., Holmström, L., Alba-Sánchez, F., Pérez-Díaz, S., Carrión, J. S., Ramos-Román, M.J., Camuera, J., Jiménez-Moreno, G., Ruha, L., Seppä, H., 2022. Spatial and temporal patterns of Holocene precipitation change in the Iberian Peninsula. Boreas 51, 776–792. https://doi.org/10.1111/bor.12586.

Imbrie, J., Berger, A., Boyle, E.A., Clemens, S.C., Duffy, A., Howard, W.R., Kukla, G., Kutzbach, J., Martinson, D.G., McIntyre, A., Mix, A.C., Molfino, B., Morley, J.J., Peterson, L.C., Pisias, N.G., Prell, W.L., Raymo, M.E., Shackleton, N.J., Toggweiler, J. R., 1993. On the structure and origin of major glaciation cycles 2. The 100,000-year cycle. Paleoceanography 8, 699–735. https://doi.org/10.1029/93PA02751.

ISPRA, 1934. Note Illustrative della Carta Geologica d'Italia alla Scala 1:100 000, Foglio 145, Avezzano. https://sgi.isprambiente.it/geologia100k/mostra_foglio.aspx?numero_foglio=145.

ISPRA, 1939. Note Illustrative della Carta Geologica d'Italia alla Scala 1:100 000, Foglio 151, Alatri. https://sgi.isprambiente.it/geologia100k/mostra_foglio.aspx?numero_foglio=151.

ISPRA, 1942. Note Illustrative della Carta Geologica d'Italia alla Scala 1:100 000, Foglio 146, Sulmona. https://sgi.isprambiente.it/geologia100k/mostra_foglio.aspx?numero_foglio=146.

ISPRA, 1967. Note Illustrative della Carta Geologica d'Italia alla Scala 1:100 000, Foglio 152, Sora. https://sgi.isprambiente.it/geologia100k/mostra_foglio.aspx?numero_foglio=152.

Jiménez-Moreno, G., Burjachs, F., Expósito, I., Oms, O., Carrancho, Á., Villalaín, J.J., Agustí, J., Campeny, G., Gómez de Soler, B., van der Made, J., 2013. Late Pliocene vegetation and orbital-scale climate changes from the western Mediterranean area. Glob. Planet. Chang. 108, 15–28. https://doi.org/10.1016/j.gloplacha.2013.05.012.

Jiménez-Moreno, G., Anderson, R.S., Markgraf, V., Staley, S.E., Fawcett, P.J., 2023. Environmental and climate evolution in the Southwest USA since the last interglacial deduced from the pollen record from Stoneman Lake, Arizona. Quat. Sci. Rev. 300, 107883 https://doi.org/10.1016/j.quascirev.2022.107883.

Joannin, S., Ciaranfi, N., Stefanelli, S., 2008. Vegetation changes during the late Early Pleistocene at Montalbano Jonico (Province of Matera, southern Italy) based on pollen analysis. Palaeogeogr. Palaeoclimatol. Palaeoecol. 270, 92–101. https://doi.org/10.1016/j.palaeo.2008.08.017.

Joannin, S., Bassinot, F., Nebout, N.C., Peyron, O., Beaudouin, C., 2011. Vegetation response to obliquity and precession forcing during the Mid-Pleistocene transition in Western Mediterranean region (ODP site 976). Quat. Sci. Rev. 30, 280–297. https://doi.org/10.1016/j.quascirev.2010.11.009.

Juggins, S., 2007. C2 Version 1.5: Software for Ecological and Palaeoecological Data Analysis and Visualisation. https://eprints.ncl.ac.uk.

Kousis, I., Koutsodendris, A., Peyron, O., Leicher, N., Francke, A., Wagner, B., Giaccio, B., Knipping, M., Pross, J., 2018. Centennial-scale vegetation dynamics and climate variability in SE Europe during marine isotope stage 11 based on a pollen record from Lake Ohrid. Quat. Sci. Rev. 190, 20–38. https://doi.org/10.1016/j.quascirev.2018.04.014.

Koutsodendris, A., 2020. Palynological Data and Pollen-Based Climate Reconstructions from Lake Ohrid during MIS 12–11. https://doi.org/10.1594/PANGAEA.915920.

Koutsodendris, A., Kousis, I., Peyron, O., Wagner, B., Pross, J., 2019. The marine isotope stage 12 pollen record from Lake Ohrid (SE Europe): investigating short-term climate change under extreme glacial conditions. Quat. Sci. Rev. 221, 105873 https://doi.org/10.1016/j.quascirev.2019.105873.

Koutsodendris, A., Dakos, V., Fletcher, W.J., Knipping, M., Kotthoff, U., Milner, A.M., Müller, U.C., Kaboth-Bahr, S., Kern, O.A., Kolb, L., Vakhrameeva, P., Wulf, S., Christanis, K., Schmiedl, G., Pross, J., 2023a. Atmospheric CO2 forcing on Mediterranean biomes during the past 500 kyrs. Nat. Commun. 14, 1664. https://doi.org/10.1038/s41467-023-37388-x.

Koutsodendris, A., Dakos, V., Fletcher, W.J., Knipping, M., Kotthoff, U., Milner, A.M., Müller, U.C., Kaboth-Bahr, S., Kern, O.A., Kolb, L., Vakhrameeva, P., Wulf, S., Christanis, K., Schmiedl, G., Pross, J., 2023b. Pollen Data from Tenaghi Philippon (Greece) Spanning the Past 500 Kyrs. https://doi.org/10.1594/PANGAEA.943593.

Kozáková, R., Šamonil, P., Kuneš, P., Novák, J., Kočár, P., Kočárová, R., 2011. Contrasting local and regional Holocene histories of *Abies alba* in the Czech Republic in relation to human impact: evidence from forestry, pollen and anthracological data. The Holocene 21, 431–444. https://doi.org/10.1177/0959683610385721.

Kuhlmann, H., Meggers, H., Freudenthal, T., Wefer, G., 2004. The transition of the monsoonal and the N Atlantic climate system off NW Africa during the Holocene. Geophys. Res. Lett. 31 https://doi.org/10.1029/2004GL021267.

Laskar, J., Robutel, P., Joutel, F., Gastineau, M., Correia, A.C.M., Levrard, B., 2004. A long-term numerical solution for the insolation quantities of the Earth. Astron. Astrophys. 428, 261–285. https://doi.org/10.1051/0004-6361:20041335.

Leicher, N., Giaccio, B., Pereira, A., Nomade, S., Monaco, L., Mannella, G., Galli, P., Peronance, E., Palladino, D.M., Sottili, G., Zanchetta, G., Wagner, B., 2023. Central Mediterranean tephrochronology between 313 and 366 ka: new insights from the Fucino palaeolake sediment succession. Boreas 52, 240–271. https://doi.org/10.1111/bor.12610.

Leicher, N., Monaco, L., Giaccio, B., Nomade, S., Pereira, A., Mannella, G., Wulf, S., Sottili, G., Palladino, D.M., Zanchetta, G., Wagner, B., 2024. Central Mediterranean tephrochronology for the time interval 250–315 ka derived from the Fucino sediment succession. Boreas 53, 164–185. https://doi.org/10.1111/bor.12637.

Li, Y., Fleitmann, D., Wang, X., Pérez-Mejías, C., Sha, L., Dong, X., Wang, D., Zhang, R., Qu, X., Cheng, H., 2023. 550-year climate periodicity in the Yunnan-Guizhou Plateau during the late Mid-Holocene: insights and implications. Geophys. Res. Lett. 50 https://doi.org/10.1029/2023GL103523 e2023GL103523.

Lionello, P., Malanotte-Rizzoli, P., Boscolo, R., Alpert, P., Artale, V., Li, L., Luterbacher, J., May, W., Trigo, R., Tsimplis, M., Ulbrich, U., Xoplaki, E., 2006. The Mediterranean climate: an overview of the main characteristics and issues. In: Lionello, P., Malanotte-Rizzoli, P., Boscolo, R. (Eds.), Developments in Earth and Environmental Sciences, Mediterranean. Elsevier, pp. 1–26. https://doi.org/10.1016/S1571-9197(06)80003-0.

Lisiecki, L.E., Raymo, M.E., 2005. A Pliocene-Pleistocene stack of 57 globally distributed benthic δ18O records. Paleoceanography 20. https://doi.org/10.1029/2004PA001071.

López-Martínez, C., Grimalt, J.O., Hoogakker, B., Gruetzner, J., Vautravers, M.J., McCave, I.N., 2006. Abrupt wind regime changes in the North Atlantic Ocean during the past 30,000–60,000 years. Paleoceanography 21. https://doi.org/10.1029/2006PA001275.

Loutre, M.F., Berger, A., 2000. Future climatic changes: are we entering an exceptionally long interglacial? Clim. Chang. 46, 61–90. https://doi.org/10.1023/A:1005559827189.

Magri, D., Tzedakis, P.C., 2000. Orbital signatures and long-term vegetation patterns in the Mediterranean. In: Quat. Int., EDLP - Med Special, 73–74, pp. 69–78. https://doi.org/10.1016/S1040-6182(00)00065-3.

Mannella, G., Giaccio, B., Zanchetta, G., Regattieri, E., Leicher, N., Scheidt, S., Grelle, T., Lehne, C., Rolf, C., Wonik, T., Nomade, S., Pereira, A., Niespolo, E., Renne, P., Leng, M., Dean, J., Thomas, C., Ariztegu, D., Gaeta, M., Florindo, F., Cavinato, G.P., Provenzale, A., Wagner, B., 2018. Fucino palaeo-lake: towards the palaeoenvironmental history of the last 430 ka. Alp. Mediterr. Quat. 31, 141–145.

Mannella, G., Giaccio, B., Zanchetta, G., Regattieri, E., Niespolo, E.M., Pereira, A., Renne, P.R., Nomade, S., Leicher, N., Perchiazzi, N., Wagner, B., 2019. Palaeoenvironmental and palaeohydrological variability of mountain areas in the central Mediterranean region: a 190 ka-long chronicle from the independently dated Fucino palaeolake record (central Italy). Quat. Sci. Rev. 210, 190–210. https://doi.org/10.1016/j.quascirev.2019.02.032.

Melles, M., Brigham-Grette, J., Minyuk, P.S., Nowaczyk, N.R., Wennrich, V., DeConto, R. M., Anderson, P.M., Andreev, A.A., Coletti, A., Cook, T.L., Haltia-Hovi, E., Kukkonen, M., Lozhkin, A.V., Rosén, P., Tarasov, P., Vogel, H., Wagner, B., 2012. 2.8 million years of Arctic climate change from Lake El'gygytgyn, NE Russia. Science 337, 315–320. https://doi.org/10.1126/science.1222135.

Monaco, L., Palladino, D.M., Gaeta, M., Marra, F., Sottili, G., Leicher, N., Mannella, G., Nomade, S., Pereira, A., Regattieri, E., Wagner, B., Zanchetta, G., Albert, P.G., Arienzo, I., D'Antonio, M., Petrosino, P., Manning, C.J., Giaccio, B., 2021. Mediterranean tephrostratigraphy and peri-Tyrrhenian explosive activity revaluated in light of the 430-365 ka record from Fucino Basin (central Italy). Earth Sci. Rev. 220, 103706 https://doi.org/10.1016/j.earscirev.2021.103706.

Monaco, L., Leicher, N., Palladino, D.M., Arienzo, I., Marra, F., Petrelli, M., Nomade, S., Pereira, A., Sottili, G., Conticelli, S., D'Antonio, M., Fabbrizio, A., Jicha, B.R., Mannella, G., Petrosino, P., Regattieri, E., Tzedakis, P.C., Wagner, B., Zanchetta, G., Giaccio, B., 2022. The Fucino 250–170 ka tephra record: new insights on peri-Tyrrhenian explosive volcanism, central Mediterranean tephrochronology, and timing of the MIS 8-6 climate variability. Quat. Sci. Rev. 296, 107797 https://doi.org/10.1016/j.quascirev.2022.107797.

Mondati, G., Spadi, M., Gliozzi, E., Cosentino, D., Cifelli, F., Cavinato, G.P., Tallini, M., Mattei, M., 2021. The tectono-stratigraphic evolution of the Fucino Basin (central Apennines, Italy): new insights from the geological mapping of its north-eastern margin. J. Maps 17, 87–100. https://doi.org/10.1080/17445647.2021.1880981.

Moreno-Amat, E., Rubiales, J.M., Morales-Molino, C., García-Amorena, I., 2017. Incorporating plant fossil data into species distribution models is not straightforward: pitfalls and possible solutions. Quat. Sci. Rev. 170, 56–68. https://doi.org/10.1016/j.quascirev.2017.06.022.

Naafs, B.D.A., Hefter, J., Stein, R., 2013. Biomarker and XRD Results for the Last 3.4 Ma from IODP Site 306-U1313. https://doi.org/10.1594/PANGAEA.818094.

Naafs, B.D.A., Hefter, J., Stein, R., 2014. Dansgaard-Oeschger forcing of sea surface temperature variability in the midlatitude North Atlantic between 500 and 400 ka (MIS 12). Paleoceanography 29, 1024–1030. https://doi.org/10.1002/2014PA002697.

Napier, T.J., Hendy, I.L., Hinnov, L.A., Brown, E.T., Shevenell, A., 2018. Subtropical hydroclimate during termination V (~430-422 ka): annual records of extreme precipitation, drought, and interannual variability from Santa Barbara Basin. Quat. Sci. Rev. 191, 73–88. https://doi.org/10.1016/j.quascirev.2018.05.003.

Nehrbass-Ahles, C., Shin, J., Schmitt, J., Bereiter, B., Joos, F., Schilt, A., Schmidely, L., Silva, L., Teste, G., Grilli, R., Chappellaz, J., Hodell, D., Fischer, H., Stocker, T.F., 2020. Abrupt CO2 release to the atmosphere under glacial and early interglacial climate conditions. Science 369, 1000–1005. https://doi.org/10.1126/science.aay8178.

Nielsen, H., Sørensen, I., 1992. Taxonomy and stratigraphy of late-glacial *Pediastrum* taxa from Lysmosen, Denmark — a preliminary study. Rev. Palaeobot. Palynol. 74, 55–75. https://doi.org/10.1016/0034-6667(92)90138-7.

Okuda, M., Yasuda, Y., Setoguchi, T., 2001. Middle to Late Pleistocene vegetation history and climatic changes at Lake Kopais, Southeast Greece. Boreas 30, 73–82. https://doi.org/10.1111/j.1502-3885.2001.tb00990.x.

Peyron, O., Magny, M., Goring, S., Joannin, S., de Beaulieu, J.-L., Brugiapaglia, E., Sadori, L., Garfi, G., Kouli, K., Ioakim, C., Combourieu-Nebout, N., 2013. Contrasting patterns of climatic changes during the Holocene across the Italian Peninsula reconstructed from pollen data. Clim. Past 9, 1233–1252. https://doi.org/10.5194/cp-9-1233-2013.

Pross, J., Christanis, K., Fischer, T., Fletcher, W.J., Hardiman, M., Kalaitzidis, S., Knipping, M., Kotthoff, U., Milner, A.M., Muller, U.C., Schmiedl, G., Siavalas, G., Tzedakis, P.C., Wulf, S., 2015. The 1.35-Ma-long terrestrial climate archive of Tenaghi Philippon, northeastern Greece: evolution, exploration, and perspectives for future research. Newsl. Stratigr. 48, 253–276. https://doi.org/10.1127/nos/2015/0063.

R Core Team, 2017. R: A Language and Environment for Statistical Computing.

Raymo, M.E., 1997. The timing of major climate terminations. Paleoceanography 12, 577–585. https://doi.org/10.1029/97PA01169.

Regattieri, E., Giaccio, B., Galli, P., Nomade, S., Peronace, E., Messina, P., Sposato, A., Boschi, C., Gemelli, M., 2016. A multi-proxy record of MIS 11–12 deglaciation and glacial MIS 12 instability from the Sulmona basin (central Italy). Quat. Sci. Rev. 132, 129–145. https://doi.org/10.1016/j.quascirev.2015.11.015.

Rodrigues, T., Voelker, A.H.L., Grimalt, J.O., Abrantes, F., Naughton, F., 2011. Iberian margin sea surface temperature during MIS 15 to 9 (580–300 ka): glacial suborbital variability versus interglacial stability. Paleoceanography 26. https://doi.org/10.1029/2010PA001927.

Rodrigues, T., Alonso-García, M., Hodell, D.A., Rufino, M., Naughton, F., Grimalt, J.O., Voelker, A.H.L., Abrantes, F., 2017. A 1-Ma record of sea surface temperature and extreme cooling events in the North Atlantic: a perspective from the Iberian margin. Quat. Sci. Rev. 172, 118–130. https://doi.org/10.1016/j.quascirev.2017.07.004.

Rohling, E.J., Braun, K., Grant, K., Kucera, M., Roberts, A.P., Siddall, M., Trommer, G., 2010. Comparison between Holocene and marine isotope stage-11 sea-level histories. Earth Planet. Sci. Lett. 291, 97–105. https://doi.org/10.1016/j.epsl.2009.12.054.

Sassoon, D., Lebreton, V., Combourieu-Nebout, N., Peyron, O., Moncel, M.-H., 2023. Palaeoenvironmental changes in the southwestern Mediterranean (ODP site 976, Alboran Sea) during the MIS 12/11 transition and the MIS 11 interglacial and implications for hominin populations. Quat. Sci. Rev. 304, 108010 https://doi.org/10.1016/j.quascirev.2023.108010.

Schmidl, A., Kofler, W., Oeggl-Wahlmüller, N., Oeggl, K., 2005. Land use in the Eastern Alps during the bronze age—an archaeobotanical case study of a hilltop settlement in the Montafon (western Austria)*. Archaeometry 47, 455–470. https://doi.org/10.1111/j.1475-4754.2005.00213.x.

Singh, H., Singh, A.D., Tripathi, R., Singh, P., Verma, K., Voelker, A.H.L., Hodell, D.A., 2023. Centennial-millennial scale ocean-climate variability in the northeastern Atlantic across the last three terminations. Glob. Planet. Chang. 223, 104100 https://doi.org/10.1016/j.gloplacha.2023.104100.

Spratt, R.M., Lisiecki, L.E., 2016. A Late Pleistocene sea level stack. Clim. Past 12, 1079–1092. https://doi.org/10.5194/cp-12-1079-2016.

Stansell, N.D., Abbott, M.B., Rull, V., Rodbell, D.T., Bezada, M., Montoya, E., 2010. Abrupt Younger Dryas cooling in the northern tropics recorded in lake sediments from the Venezuelan Andes. Earth Planet. Sci. Lett. 293, 154–163. https://doi.org/10.1016/j.epsl.2010.02.040.

Ter Braak, C., Juggins, S., 1993. Weighted averaging partial least squares regression (WA-PLS): definition and comparison with other methods for species-environment calibration. In: Patil, G.P., Rao, C.R. (Eds.), Multivariate Environmental Statistics, pp. 525–560.

Tomassetti, B., Giorgi, F., Verdecchia, M., Visconti, G., 2003. Regional model simulation of the hydrometeorological effects of the Fucino Lake on the surrounding region. Ann. Geophys. 21, 2219–2232. https://doi.org/10.5194/angeo-21-2219-2003.

Tzedakis, P.C., 2007. Seven ambiguities in the Mediterranean palaeoenvironmental narrative. Quat. Sci. Rev. 26, 2042–2066. https://doi.org/10.1016/j.quascirev.2007.03.014.

Tzedakis, P.C., 2010. The MIS 11 / MIS 1 analogy, southern European vegetation, atmospheric methane and the "early anthropogenic hypothesis". Clim. Past 6, 131–144. https://doi.org/10.5194/cp-6-131-2010.

Tzedakis, P.C., Bennett, K.D., 1995. Interglacial vegetation succession: a view from southern Europe. Quat. Sci. Rev. 14, 967–982. https://doi.org/10.1016/0277-3791(95)00042-9.

Tzedakis, P.C., Andrieu, V., de Beaulieu, J.-L., Crowhurst, S., Follieri, M., Hooghiemstra, H., Magri, D., Reille, M., Sadori, L., Shackleton, N.J., Wijmstra, T.A., 1997. Comparison of terrestrial and marine records of changing climate of the last 500,000 years. Earth Planet. Sci. Lett. 150, 171–176. https://doi.org/10.1016/S0012-821X(97)00078-2.

Tzedakis, P.C., Raynaud, D., McManus, J.F., Berger, A., Brovkin, V., Kiefer, T., 2009. Interglacial diversity. Nat. Geosci. 2, 751–755. https://doi.org/10.1038/ngeo660.

Tzedakis, P.C., Hodell, D.A., Nehrbass-Ahles, C., Mitsui, T., Wolff, E.W., 2022. marine isotope stage 11c: an unusual interglacial. Quat. Sci. Rev. 284, 107493 https://doi.org/10.1016/j.quascirev.2022.107493.

Vázquez Riveiros, N., Waelbroeck, C., Skinner, L., Duplessy, J.-C., McManus, J.F., Kandiano, E.S., Bauch, H.A., 2013. The "MIS 11 paradox" and ocean circulation: role of millennial scale events. Earth Planet. Sci. Lett. 371–372, 258–268. https://doi.org/10.1016/j.epsl.2013.03.036.

Wagner, B., Vogel, H., Francke, A., Friedrich, T., Donders, T., Lacey, J.H., Leng, M.J., Regattieri, E., Sadori, L., Wilke, T., Zanchetta, G., Albrecht, C., Bertini, A., Combourieu-Nebout, N., Cvetkoska, A., Giaccio, B., Grazhdani, A., Hauffe, T., Holtvoeth, J., Joannin, S., Jovanovska, E., Just, J., Kouli, K., Kousis, I., Koutsodendris, A., Krastel, S., Lagos, M., Leicher, N., Levkov, Z., Lindhorst, K., Masi, A., Melles, M., Mercuri, A.M., Nomade, S., Nowaczyk, N., Panagiotopoulos, K., Peyron, O., Reed, J.M., Sagnotti, L., Sinopoli, G., Stelbrink, B., Sulpizio, R., Timmermann, A., Tofilovska, S., Torri, P., Wagner-Cremer, F., Wonik, T., Zhang, X., 2019. Mediterranean winter rainfall in phase with African monsoons during the past 1.36 million years. Nature 573, 256–260. https://doi.org/10.1038/s41586-019-1529-0.

Wang, M., Zheng, H., Xie, X., Fan, D., Yang, S., Zhao, Q., Wang, K., 2011. A 600-year flood history in the Yangtze River drainage: comparison between a subaqueous delta and historical records. Chin. Sci. Bull. 56, 188–195. https://doi.org/10.1007/s11434-010-4212-2.

Xiang, L., Huang, X., Huang, C., Chen, X., Wang, H., Chen, J., Hu, Y., Sun, M., Xiao, Y., 2021. Pediastrum (Chlorophyceae) assemblages in surface lake sediments in China and western Mongolia and their environmental significance. Rev. Palaeobot. Palynol. 289, 104396 https://doi.org/10.1016/j.revpalbo.2021.104396.